



CHAPTER V

METAL RECOVERY BY ELECTROPRECIPITATION TECHNIQUE

In the previous chapter, the result of metal recovery obtained by electrodeposition technique was presented. It has been demonstrated that this technique is efficient for the copper and zinc recovery. However, due to the requirement of specific conditions and a low current efficiency in electrodeposition of some metals such as chromium or nickel, another technique is applied to remove and recover these heavy metals from aqueous solutions. This chapter deals with chromium and nickel recovery by using electroprecipitation technique with a membrane reactor. After obtaining experimental results, model of this process in terms of pH evolution in cathodic compartment and many assumptions was developed and its estimation was also compared with experimental results.

1. Chromium recovery

The electrodeposition technique is not effective in recovering chromium because it needs a specific condition ($\text{H}_2\text{SO}_4/\text{CrO}_3 = 1/100$ by weight). The suitable technique to recover chromium will be the electroprecipitation technique. Chromium ions in solution are reacted with hydroxide ion at suitable pH and then precipitated as chromium hydroxide. Experiments were performed in a reactor with membrane as presented in Chapter III (Figure III.5). The reactor was separated to two compartments by anionic membrane (IONAC, surface area of 7744 mm^2 type IONAC). Two pumps were used to circulate an electrolyte at both sides of reactor. The solution descriptions and operating conditions were detailed in Tables III.2 and III.4, respectively.

1.1 Influence of current density

Figures V.1 and V.2 show the percentage of chromium recovery as a function of time at a current density range from 90 to 203 A/m^2 for solutions S4 (pH = 1) and S5 (pH = 4.6).

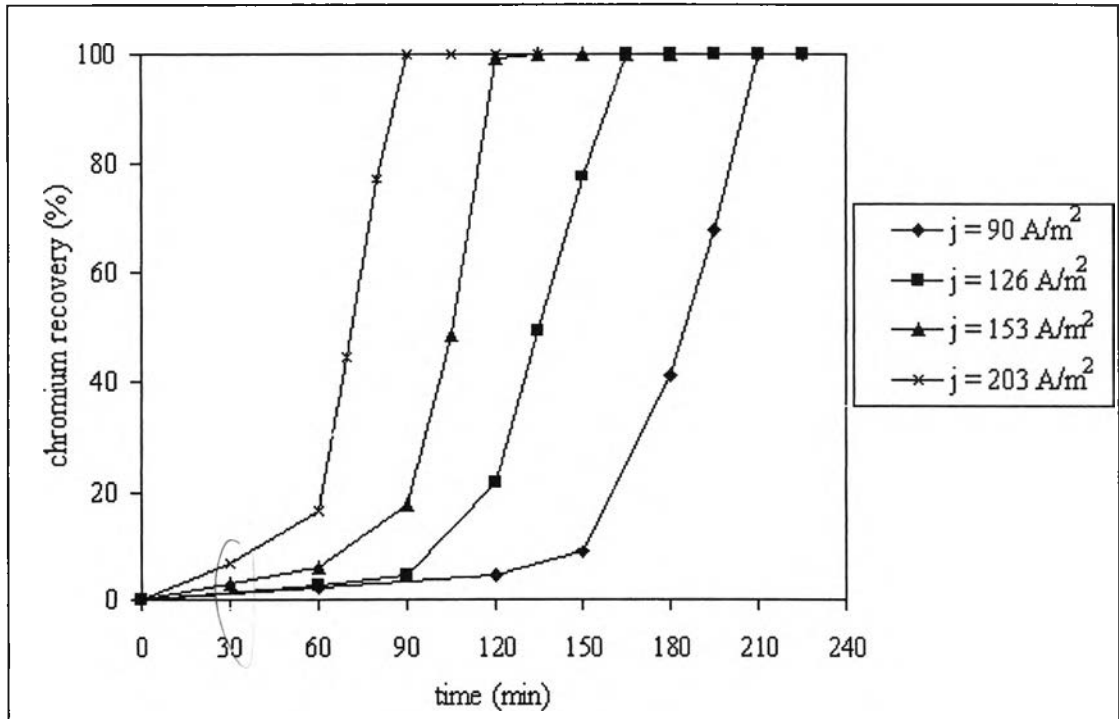


Figure V.1: Chromium recovery percentage versus time (solution S4).

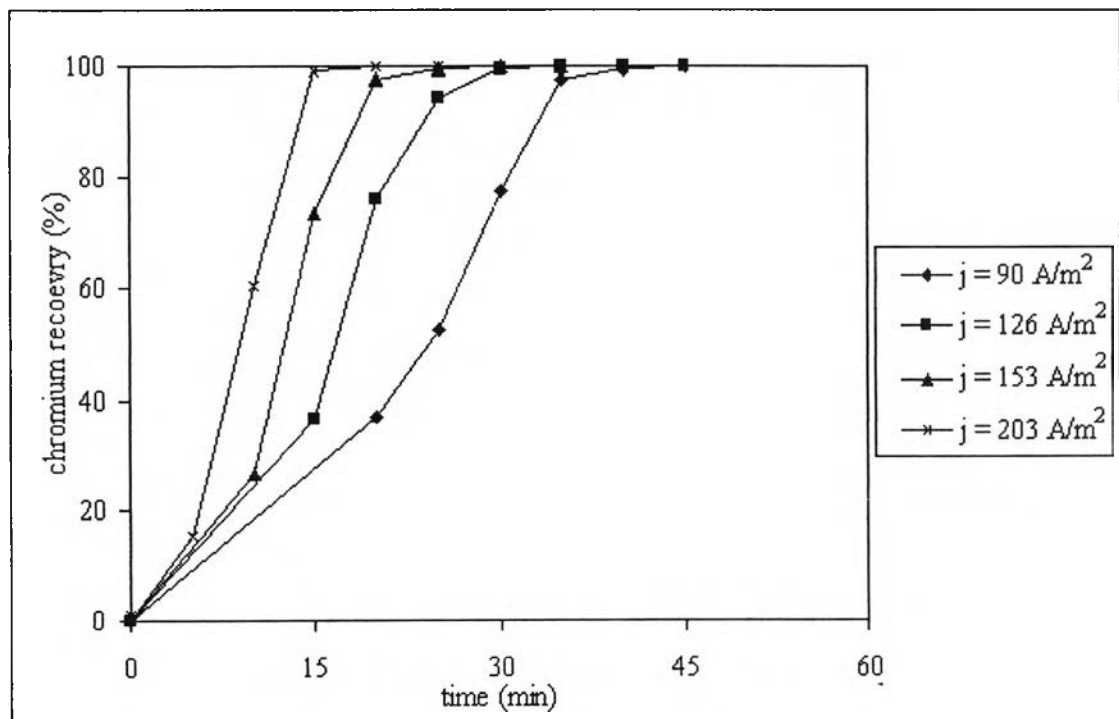


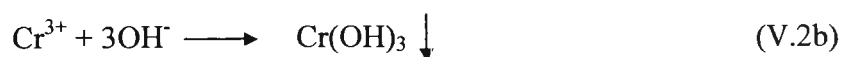
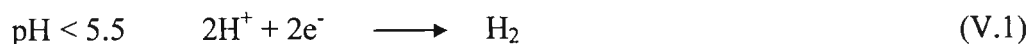
Figure V.2: Chromium recovery percentage versus time (solution S5).

The results showed that the chromium was completely recovered at every current densities. The operating time was an inverse function with current density. It decreased with increasing in current density. This is because a high current density conducts a large amount of electrons supplied to the system.

Comparing the complete precipitation time of both pH solutions, the time used for solution S5 was less than that used for solution S4 under the same current density. It is obvious that solution S5 had a high initial pH so the time to decrease proton concentrations in this solution was short.

The percentage of chromium recovery, cathodic pH and anodic pH evolution are plotted versus electrolysis time at a current density ranging from 90 to 203 A/m² at initial pH solutions of 1 and 4.6 respectively shown in Figures V.3 and V.4. In the cathodic compartment, pH increased slightly with a little difference from initial pH by the reduction reaction of proton to hydrogen gas and hydroxide ions (equation (V.1)). During this period, the chromium recovery percentage was also low. pH of solution increased continuously until the solution pH reached about 5.5 by equation (V.2a). Then, the precipitation of chromium occurred with hydroxide ions produced in the system (equation (V.2b)). At this point, pH of solution must be constant or has a little change until the precipitation of chromium is completed. After that, pH in this compartment increased rapidly due to water reduction reaction (equation (V.3)). In the anodic compartment, the oxidation reaction was taken place to convert water to oxygen gas and protons (equation (V.4)) so that pH in this compartment was diminished gradually. The observed reactions in both compartments were expressed by

Reactions in the cathodic compartment



Reactions in the anodic compartment

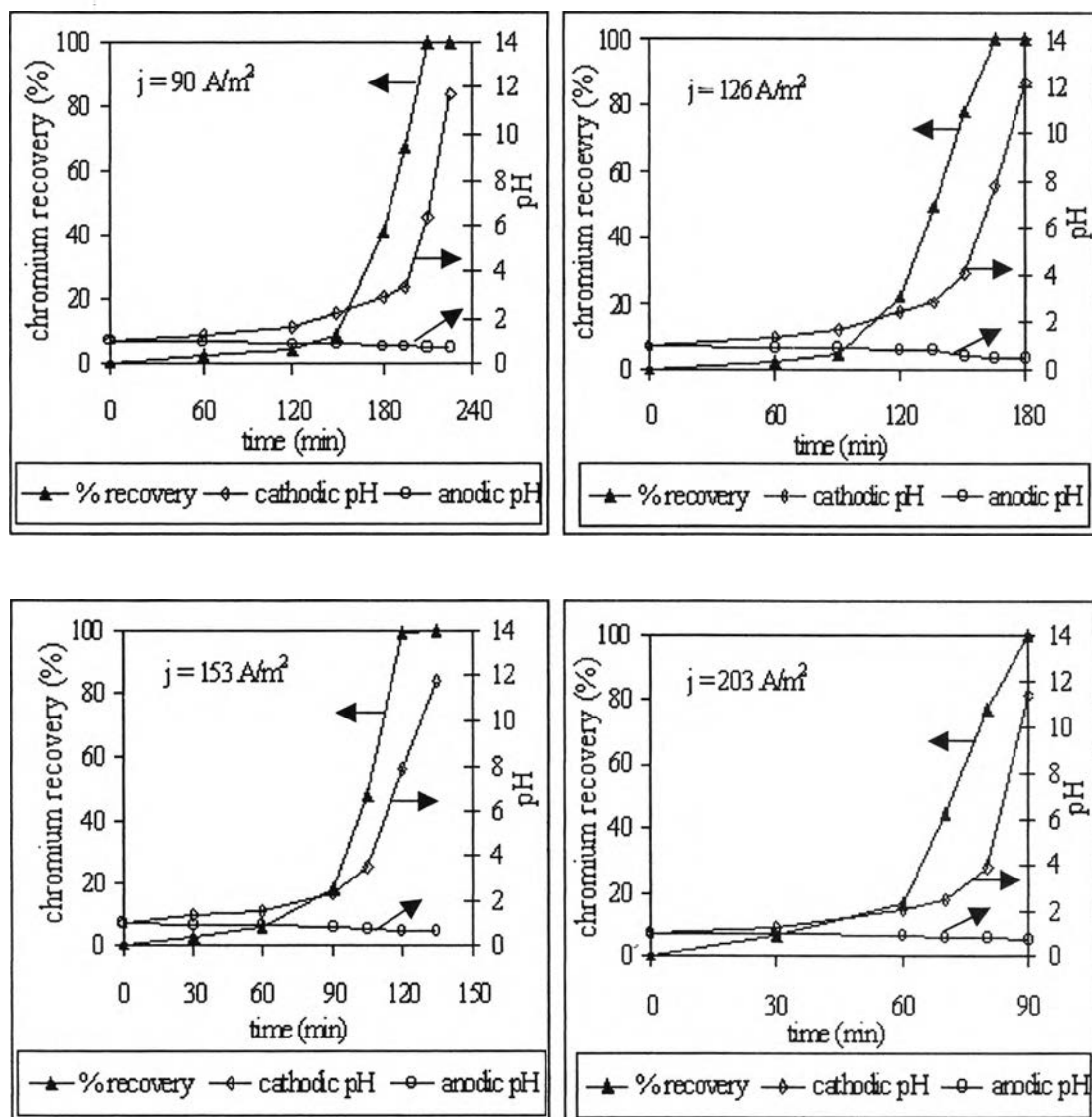


Figure V.3: Chromium recovery percentage and pH versus time (solution S4).

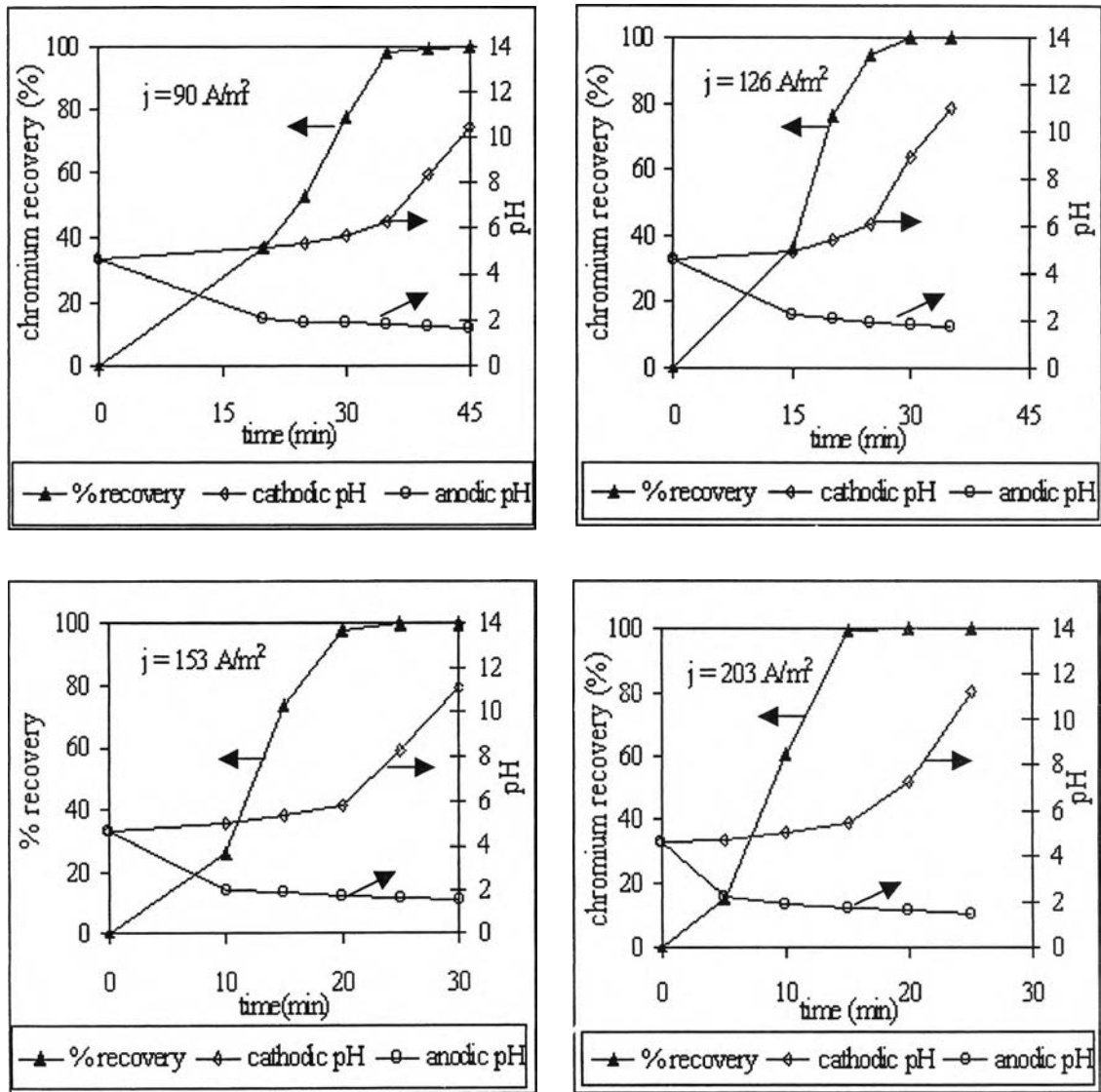


Figure V.4: Chromium recovery percentage and pH versus time (solution S5).

Figures V.5 and V.6 show operating cost versus the electrical current density for solution S4 and S5, respectively. The correlation was expressed as

$$\text{Operating cost} = f(\text{current density, electrolysis time}) \tag{V.5}$$

Operating costs for chromium solution of pH = 1 were about 3.23 US\$/m³ and about 0.72 US\$/m³ for pH = 4.6. It indicates that a high initial pH solution leads to a lower operating cost because of a shorter recovery time.

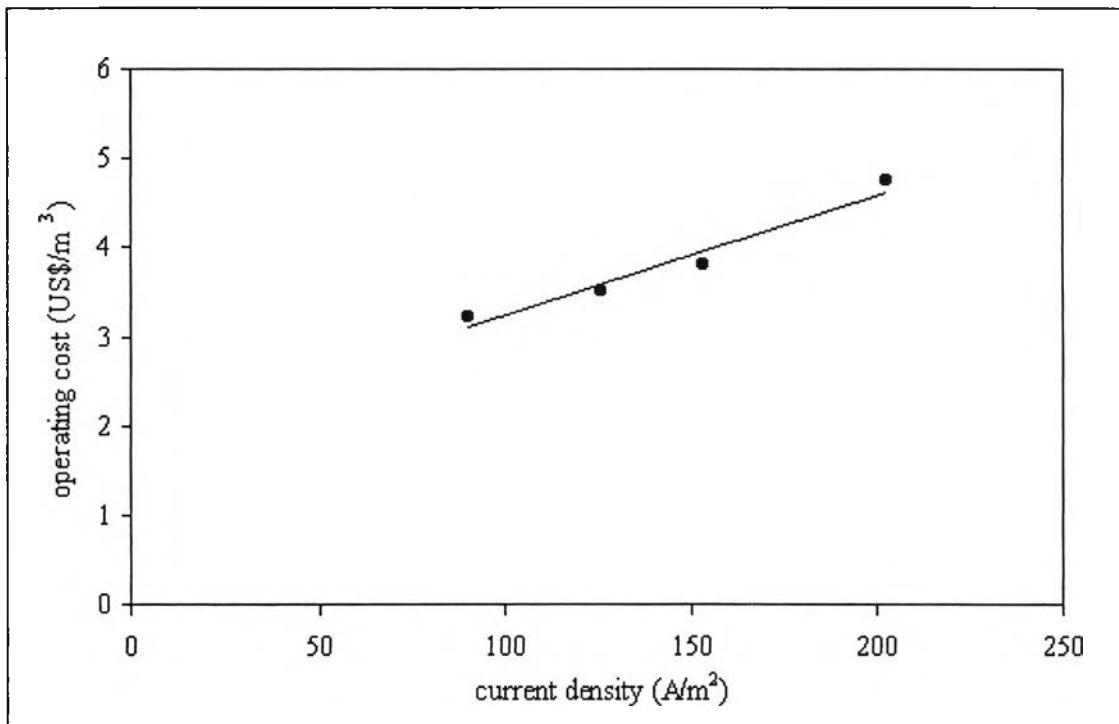


Figure V.5: Operating cost versus current density (solution S4).

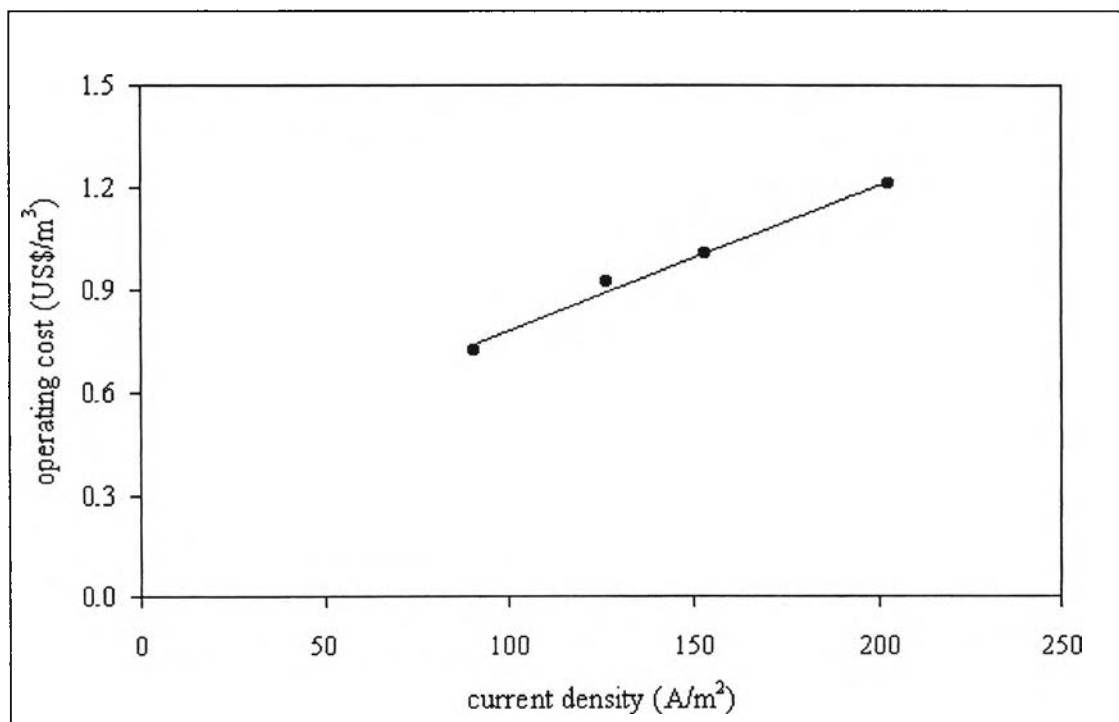


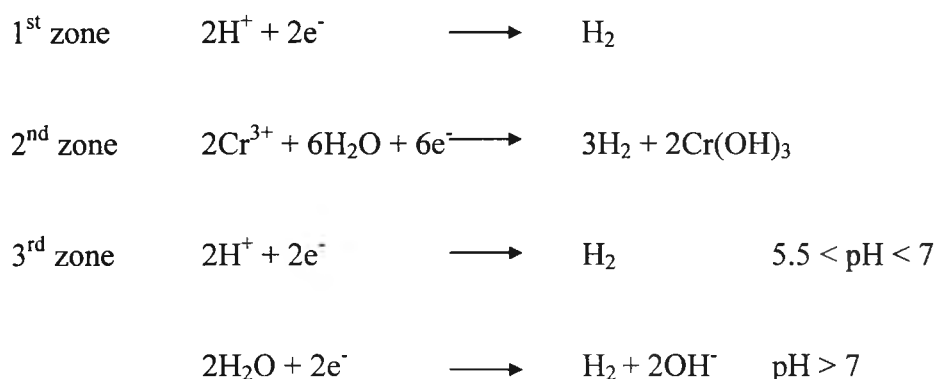
Figure V.6: Operating cost versus current density (solution S5).

Decreasing of current density may give a lower operating cost but a longer operating time. This is not agreed with economic reason. Then, the experiments were not performed at a current density lower than the minimum previous current density. For the continuous experiments, the operating current density will be performed at 90 A/m².

1.2 Model for chromium recovery

In this work, three models for chromium recovery have been developed depending upon different assumptions to predict the pH evolution in the cathodic compartment and to compare with experimental pH evolution.

The precipitation time is separated in three zones, 1st, 2nd and 3rd zone, depending on the observed reaction. The following equations present the reactions used in models.



The observed reaction in the first zone of electrolysis time is the reduction reaction of protons to hydrogen gas. The precipitation of chromium with hydroxide ions which is produced by water reduction reaction was observed in the second zone of electrolysis time. Finally, in the third zone, the reduction reactions of residual protons and water were noted after complete precipitation was reached.

1.2.1 The basic model

This model was based on two assumptions. The first one is that the precipitation of chromium occurs at constant pH (pH = 5.5). The another is that there is no hydroxide ion loss from the cathodic compartment to the anodic one. Followed these assumptions and previous reactions, the modelling equations have been modified and expressed by

$$1^{st}: pH_{sol} < 5.5, [Cr^{3+}] > 0, t < t_1, t_1 = 10^{-pH} \frac{nFV}{i}$$

$$pH_{m1} = -\log \left[10^{-pH} - \left(\frac{it}{nFV} \right) \right] \quad (V.6)$$

$$2^{nd}: pH_{sol} = 5.5, [Cr^{3+}] > 0, t_1 < t < t_2, t_2 = t_1 + \frac{3nFV[Cr]}{52i}$$

$$pH_{m1} = 5.5 \quad (V.7)$$

$$3^{rd}: pH_{sol} > 5.5, [Cr^{3+}] = 0, t > t_2$$

$$pH_{m1} = -\log \left[10^{-14} \frac{nFV}{i(t-t_2)} \right] \quad (V.8)$$

In the first period, the pH of solution (pH_{m1}) increased from initial pH to pH = 5.5 followed the 1st zone equation, and chromium ions started to precipitate at the beginning of the 2nd zone equation. During this period, pH remained constant at 5.5 until chromium precipitation was complete. Then, pH increased rapidly due to protons and water reduction reactions.

Figure V.7 displays the plots of experimental pH (pH_{exp}) and the first model pH (pH_{m1}) versus electrolysis time of synthetic chromium solution (Solution S4, pH = 1) at current density of 90 - 203 A/m². The great difference between pH_{exp} and pH_{m1} evolution was observed. The former evolution needs longer electrolysis time than the latter evolution. On the other hand, when an experiment started with high initial pH solution (Solution S5), a good agreement between experimental and calculated pH evolution was obtained (Figure V.8).

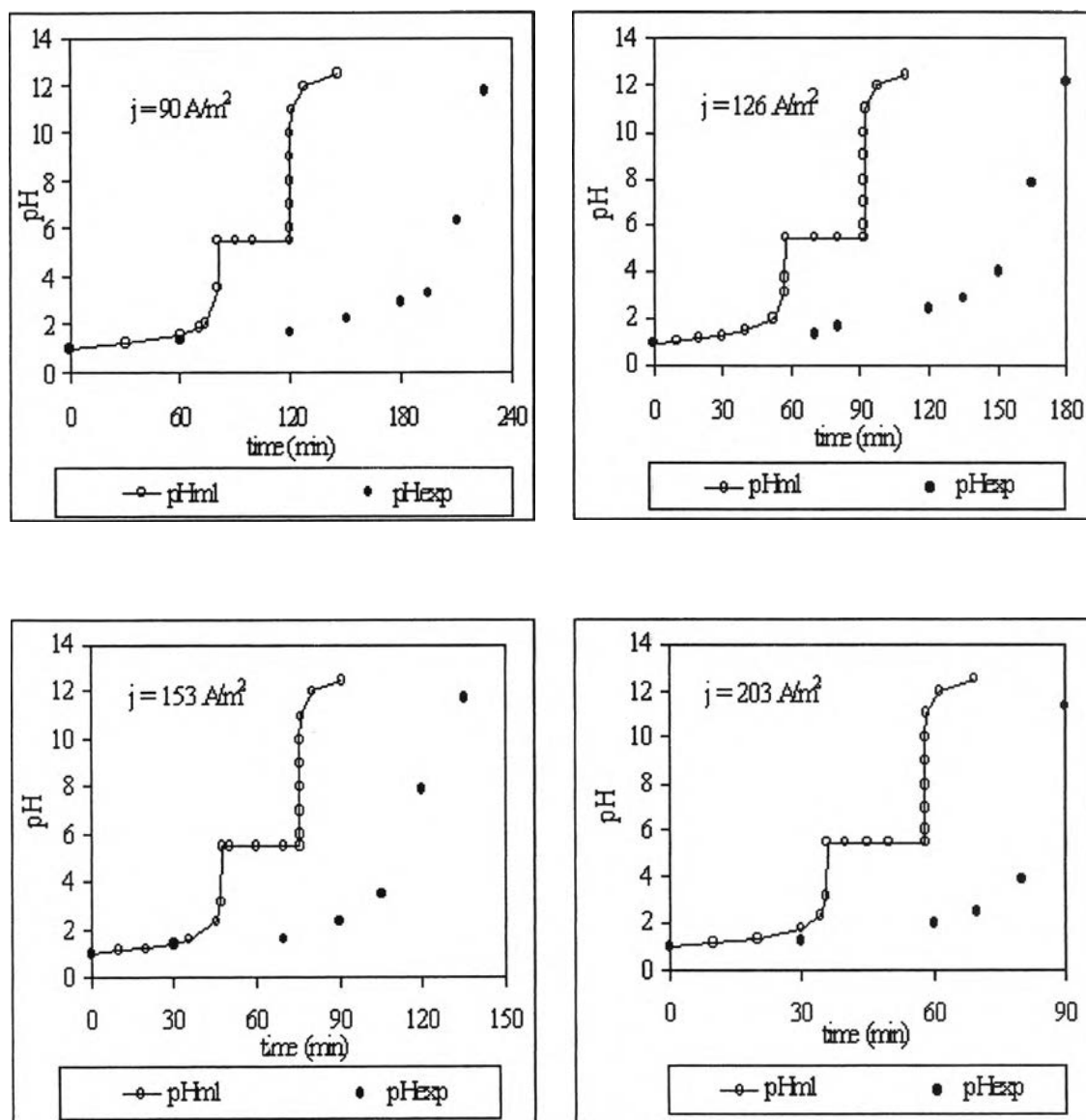


Figure V.7: Comparison between pH_{exp} and pH_{m1} evolution versus time (solution S4).

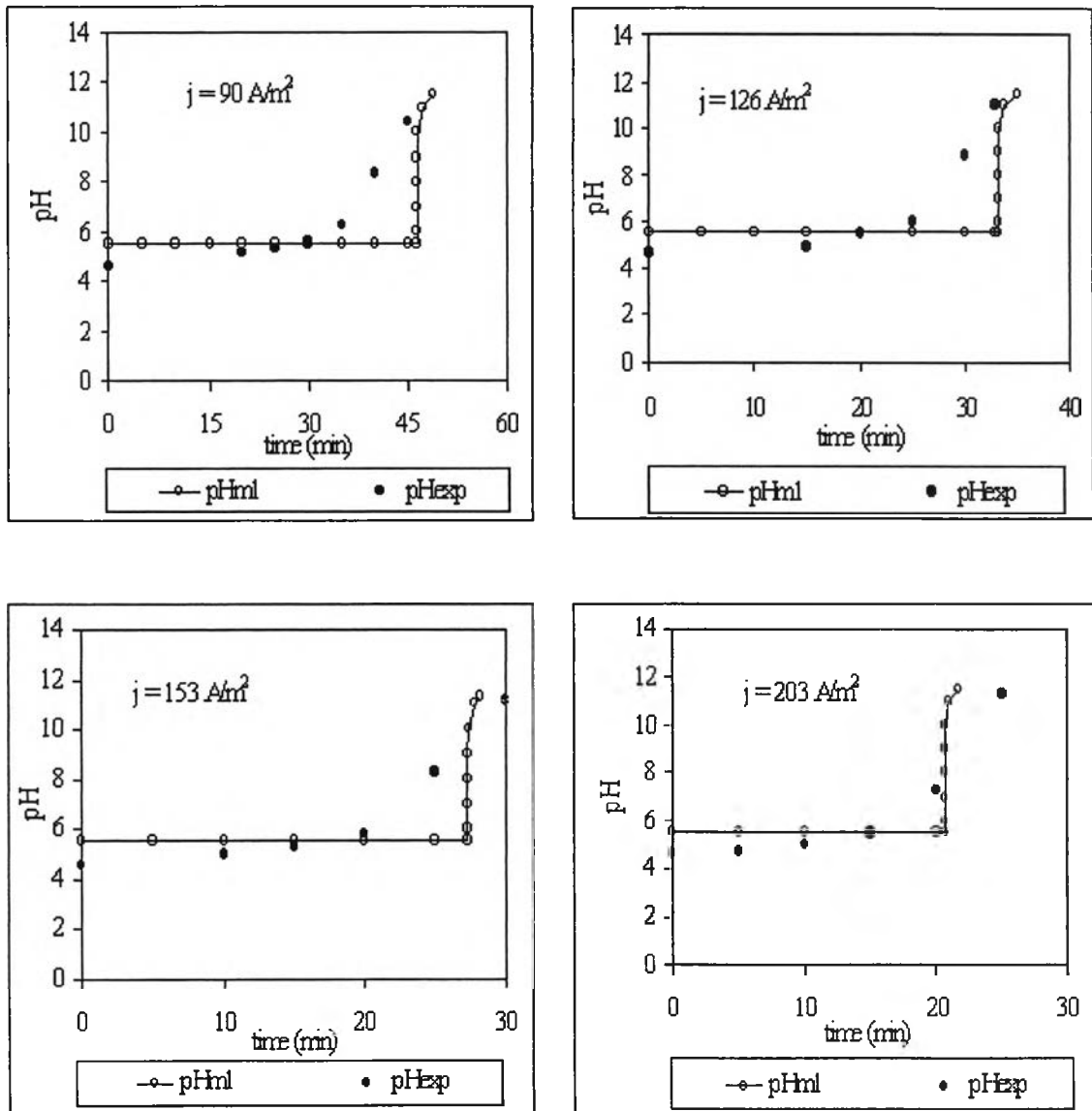


Figure V.8: Comparison between pH_{exp} and pH_{m1} evolution versus time (solution S5).

1.2.2 Non - constant pH precipitation model

The supplementary assumption of the second model is that chromium precipitates at non - constant pH. The precipitation data for this model came from both references and experiments. Three references were included in this model [60, 61, 62]. For the data of experiment, it was investigated by adding sodium hydroxide (NaOH) in synthetic chromium solution, analysing the concentration of chromium by using Atomic Absorption Spectrophotometer, and measuring the pH. Figure V.9 reviews the chromium precipitation curves at different pH. The results showed that chromium precipitation data differed from other works and solubility data.

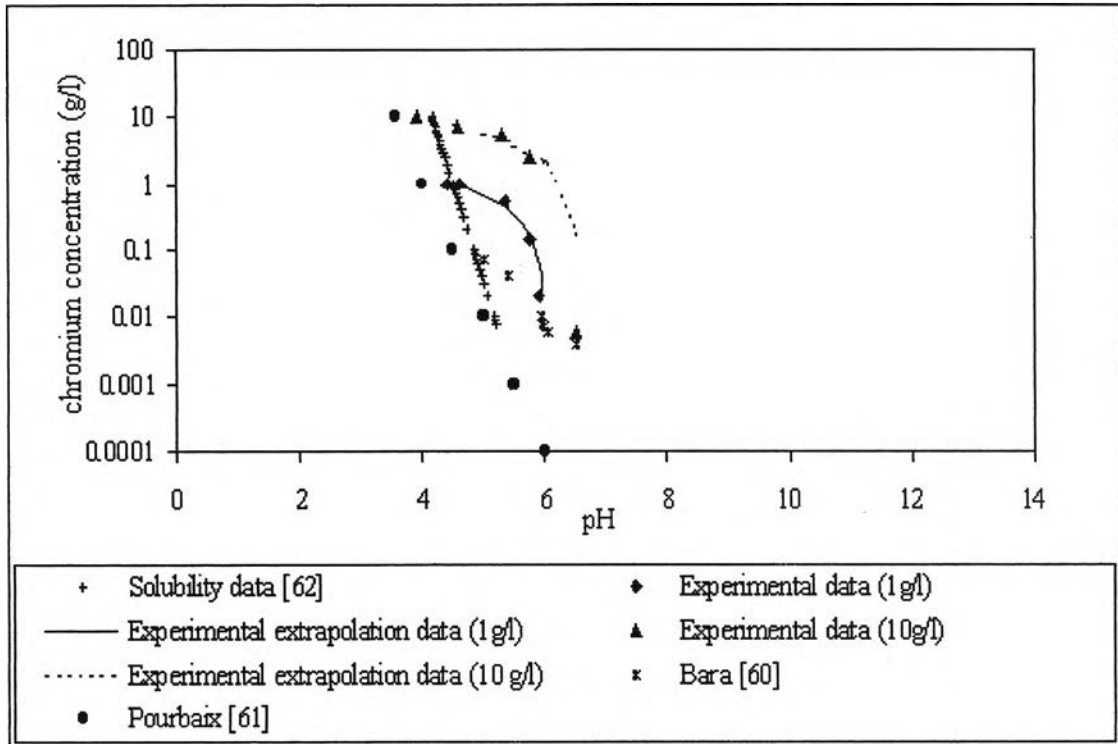


Figure V.9: Precipitation data of chromium solution.

These precipitation data were included in this model, the chromium concentration depending upon the pH has been written as the following equations.

$$\text{Experimental data: } pH_{\text{exp}} = \frac{[Cr] - 4.01}{-0.67} \quad (\text{V.9})$$

$$\text{Pourbaix data: } pH_{\text{Pourbaix}} = 4 - 0.217 \ln[Cr] \quad (\text{V.10})$$

$$\text{Solubility data: } pH_{k_{sp}} = -\log k_w \left(\frac{[Cr]}{M_w k_{sp}} \right)^{\frac{1}{3}} \quad (\text{V.11})$$

Where the solubility constant of water is 10^{-14} and the chromium solubility constant is 6.31×10^{-31} .

Similar to the first model, three pH zones versus electrolysis time have been used. The reactions observed in each zone were similar to these presented in the first model. For the first and the third zone, model equations were exactly the same.

However, for the second zone, the precipitation data were included in the model equation to predict the pH evolution during the precipitation period.

$$1^{st}: [Cr^{3+}] > 0, \quad t < t_1; \quad t_1 = 10^{-pH_i} \frac{nFV}{i}$$

$$pH_{m2} = -\log_{10} \left[10^{-pH_i} - \left(\frac{it}{nFV} \right) \right] \quad (V.12)$$

$$2^{nd}: [Cr^{3+}] > 0, \quad t_1 < t < t_2; \quad t_2 = t_1 + \frac{3nFV[Cr]}{52i}$$

$$pH_{m2-exp} = \left[4.01 + \frac{52i(t-t_1)}{3nFV} - [Cr] \right] / 0.67 \quad (V.13)$$

$$pH_{m2-Pourbaix} = 4 - 0.217 \ln \left[[Cr] - \frac{52i(t-t_1)}{3nFV} \right] \quad (V.14)$$

$$pH_{m2-k_{sp}} = -\log k_w \left(\frac{\left([Cr] - \frac{52i(t-t_1)}{3nFV} \right)^{1/3}}{52 k_{sp}} \right) \quad (V.15)$$

$$3^{rd}: [Cr^{3+}] = 0, \quad t > t_2$$

$$pH_{m2} = -\log \left[10^{-14} \frac{nFV}{i(t-t_2)} \right] \quad (V.16)$$

where pH_{m2-exp} , $pH_{m2-Pourbaix}$ and $pH_{m2-k_{sp}}$ are the pH evolution given by the second model of the experimental data, Pourbaix data and solubility data, respectively.

At initially, the calculated pH (pH_{m2}) increased from initial pH as given by the 1st zone equation and chromium ions started to precipitate as following the equation expressed in the 2nd zone. During precipitating, the pH was not constant as shown in the first model, change in pH depends upon chromium concentration as expressed in

equations (V.9) to (V.11). Finally, pH rapidly increased to the maximum pH due to proton and water reduction reactions as equation given in the 3rd zone.

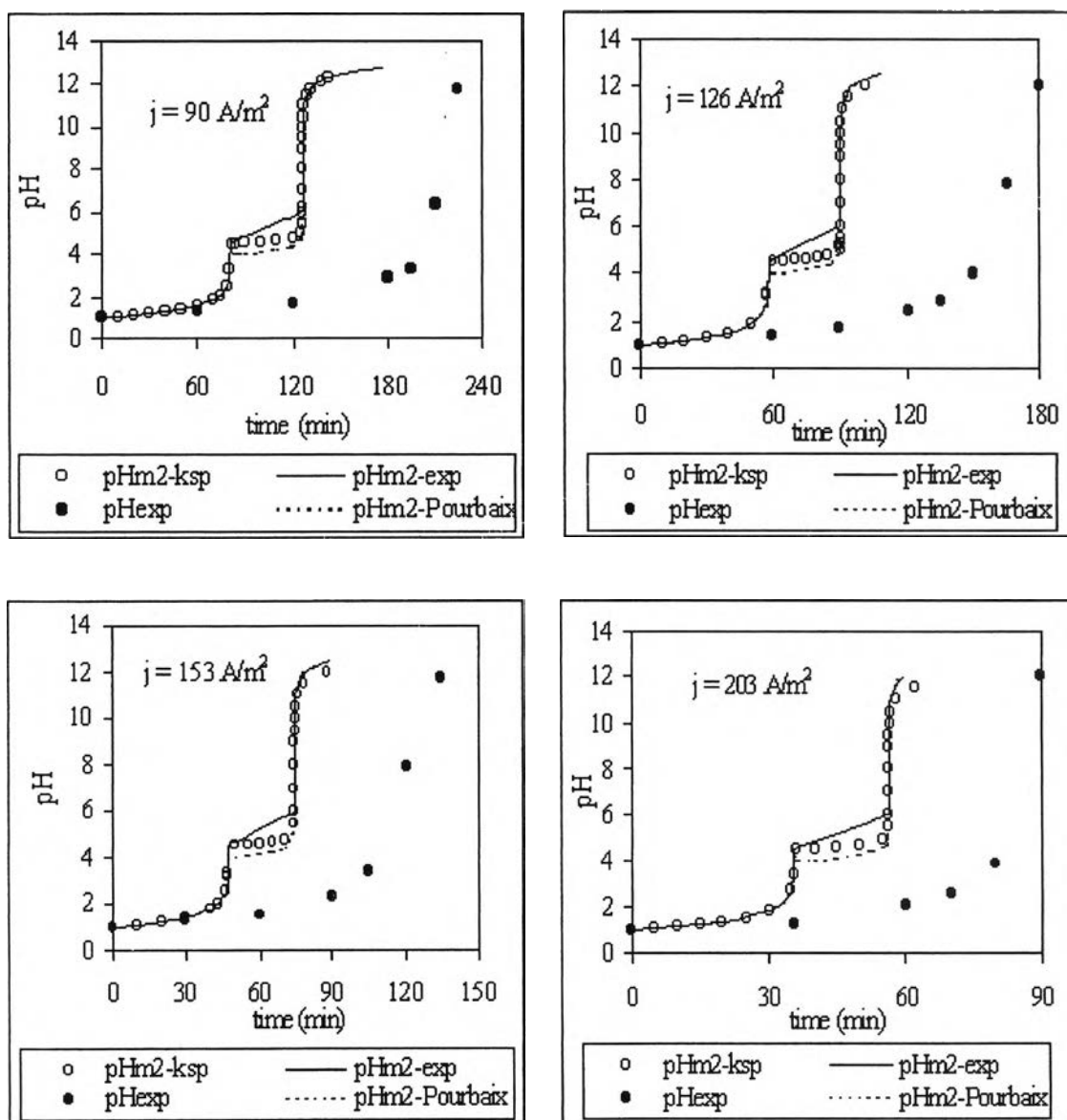


Figure V.10: Comparison between pH_{exp} and pH_{m2} evolution versus time (solution S4).

Figures V.10 and V.11 show the results of the second model comparing to experimental pH evolution of synthetic chromium solutions at pH = 1 and pH = 4.6. It showed that although the different precipitation data were included, large difference between experimental and calculated pH evolution were always observed for solution S4 at pH = 1. These differences remain similar to the results of the first model. It indicates that these differences do not come from the precipitation data used. However, similar to the previous model, the good fitting between experimental and

calculated pH evolution was obtained at $\text{pH} = 4.6$. A few differences were observed when the increasing of solution pH occurred rapidly due to non homogeneous of pH between electrode surface and bulk solution.

As the first calculation, it could be said that the two preliminary models were not sufficient to describe experimental pH for solutions with initial $\text{pH} = 1$, so another model with more assumptions has been investigated.

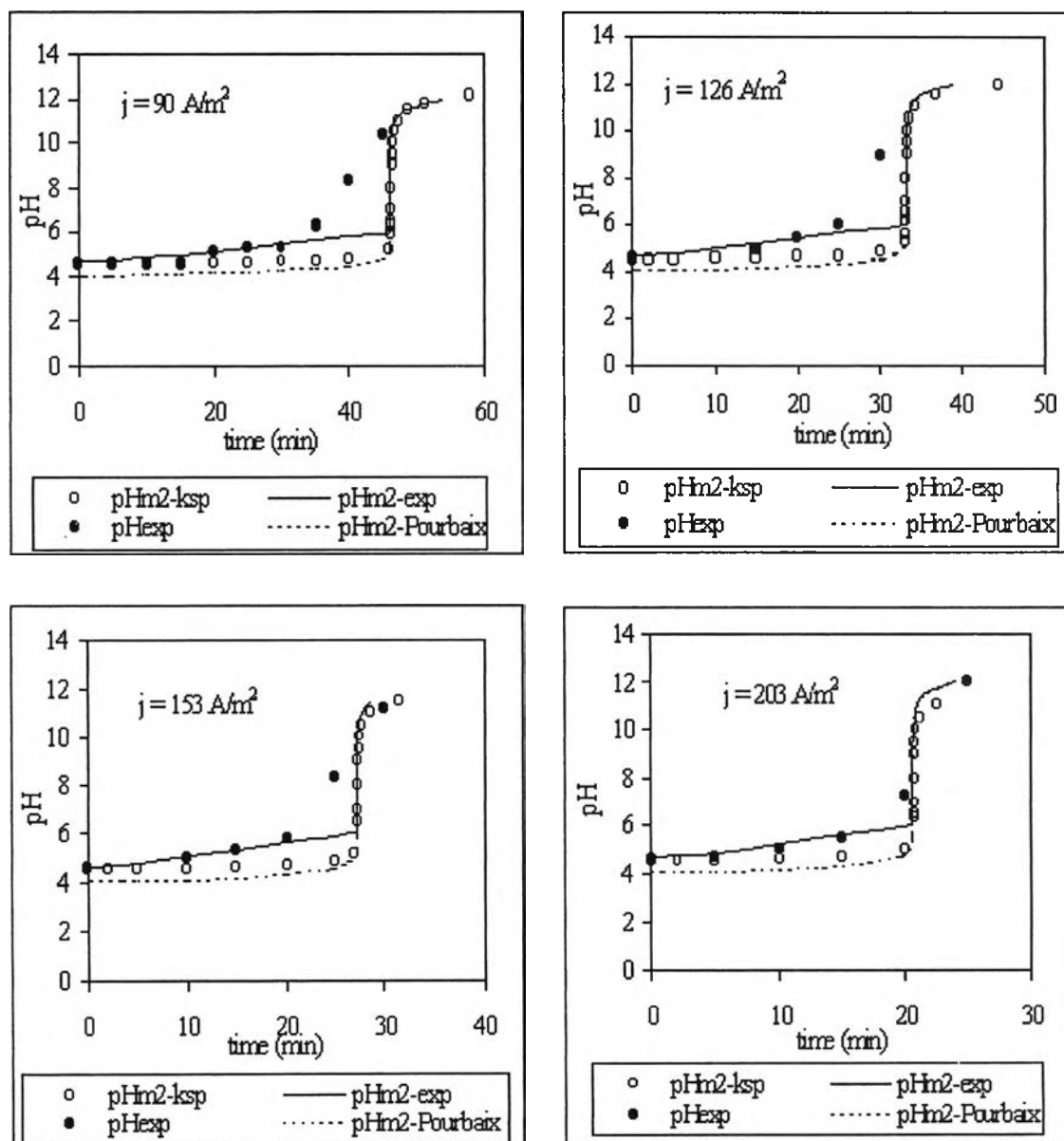


Figure V.11: Comparison between pH_{exp} and pH_{m2} evolution versus time (solution S5).

1.2.3 Non - constant pH precipitation with loss flux of hydroxide ion model

Assumptions of this model are that chromium precipitates at non - constant pH and the system lost flux of hydroxide ions from cathodic to anodic compartments. In the first time, this loss flux through the membrane has been established by material balance between anodic and cathodic compartments of proton consumption which is normally equilibrium with amount of hydroxide ions. The calculation of material balance was shown in Appendix A.6. Table V.1 shows results of material balance in terms of proton loss flux (N_{H^+}).

Table V.1: Material balance of proton in chromium precipitation process.

Current density, (A/m ²)	N_{H^+} in cathodic part (mol/m ² s)	N_{H^+} in anodic part (mol/m ² s)	N_{H^+} average (mol/m ² s)
90	1.02×10^{-3}	0.73×10^{-3}	0.88×10^{-3}
126	1.41×10^{-3}	1.16×10^{-3}	1.29×10^{-3}
153	1.65×10^{-3}	1.27×10^{-3}	1.46×10^{-3}
203	2.17×10^{-3}	1.65×10^{-3}	1.91×10^{-3}

A presence of proton flux in cathodic compartment indicated the amount of proton that should be reacted precisely with the hydroxide ion produced in this compartment or, in the other hand, the same amount of hydroxide ion is loss from this compartment. As the same manner, the flux of proton in the anodic compartment demonstrates the loss of proton from this compartment. This loss is caused by the reaction with hydroxide ion coming from the cathodic compartment.

The results of proton balance showed the differences exist between estimated values in anodic and cathodic compartments. Due to these phenomenon, three values of proton loss flux (N_{H^+}) estimated from cathodic compartment, anodic compartment and average values were substituted in the third model in order to find the best correlation with experimental results. Similar to two previous models, the equations of the third model were classified into three zones versus electrolysis time. The equation modified by our experiment was included in this model during the precipitation zone. In addition, the precipitation is quickly so no hydroxide ions loss flux will be consider during this zone. The third model equations were

$$1^{st}: [Cr^{3+}] > 0, \quad t < t_1; \quad t_1 = 10^{-pH_1} \left(\frac{i}{nFV} - \frac{N_{H^+}A}{V} \right)$$

$$pH_3 = -\log \left[10^{-pH_1} - \frac{it}{nFV} + \frac{N_{H^+}At}{V} \right] \quad (V.17)$$

$$2^{nd}: [Cr^{3+}] > 0, \quad t_1 < t < t_2; \quad t_2 = t_1 + \frac{3nFV[Cr]}{52i}$$

$$pH_{m3} = \left[4.01 + \frac{52i(t-t_1)}{3nFV} - [Cr] \right] / 0.67 \quad (V.18)$$

$$3^{rd}: [Cr^{3+}] = 0, \quad t > t_2$$

$$pH_{m3} = -\log \left[\frac{10^{-14}}{(t-t_2) \left[\frac{i}{nFV} - \frac{N_{H^+}A}{V} \right]} \right] \quad (V.19)$$

The comparison between experimental pH (pH_{exp}) and model pH (pH_{m3}) calculated by the third model equation is shown in Figure V.12. The loss flux used in the third model composed of the loss flux from the anodic compartment (pH_{m3-NA}), the loss flux from the cathodic compartment (pH_{m3-NC}) and an average of loss flux from two compartments (pH_{m3-Nav}).

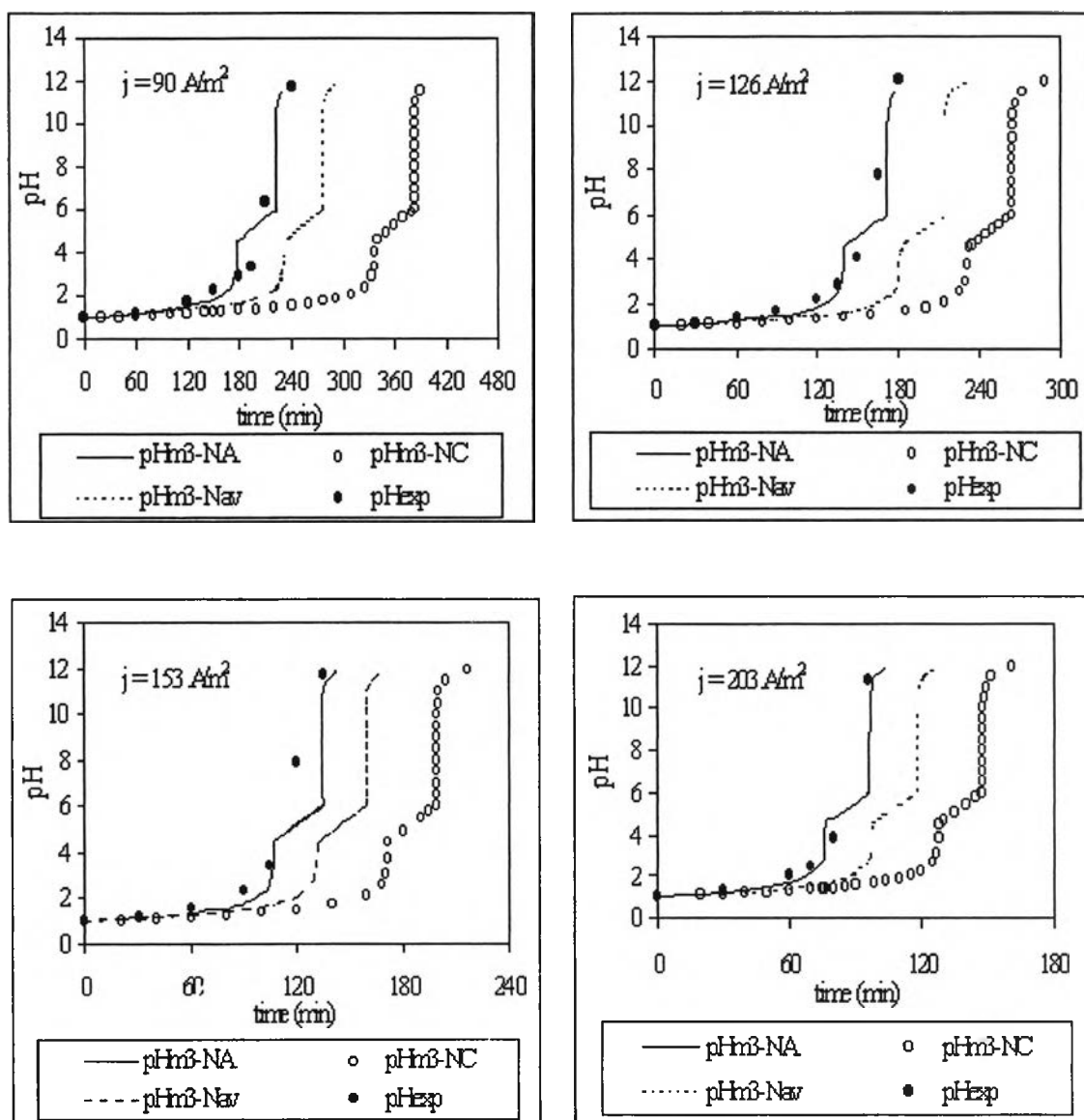


Figure V.12: Comparison between pH_{exp} and pH_{m3} evolution versus time(solution S4).

The experimental results and model predictions had a similar behaviour when a current density was applied. It is marked that the experimental result had a good fitting to that from the anodic compartment at which only proton reduction occurred. It did not fit to the results from the cathodic compartment at which water and proton reduction occurred. By this reason, the current efficiency in cathodic compartment is not 100 % as our assumption so the exact value of loss flux is not obtained. On the other hand, in anodic compartment, only one reaction happened so the high precision of loss flux is obtained.

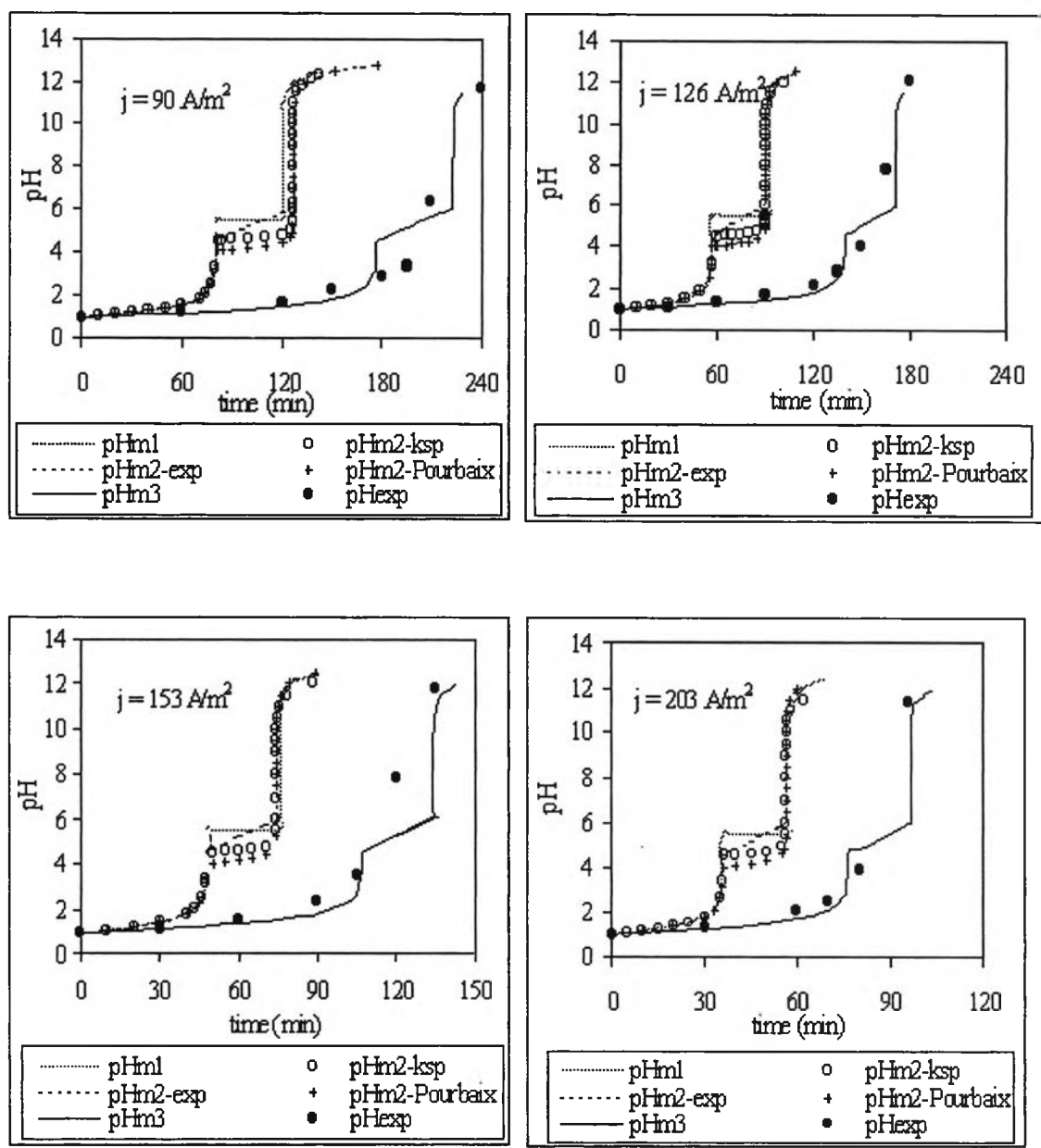


Figure V.13: Plots of pH_{m1} , pH_{m2} , pH_{m3} and pH_{exp} evolution versus time (solution S4).

The plots of experimental results and pH evolution in cathodic compartment calculated by the first, the second, the third models versus electrolysis time of solutions S4 and S5 are shown respectively in Figures V.13 and V.15. The concentration evolutions of the developed model and experiment are plotted in Figures V.14 and V.16 for solutions S4 and S5, respectively. The results showed that the third model gave the best fitting with experimental pH and concentration evolution for the both solutions.

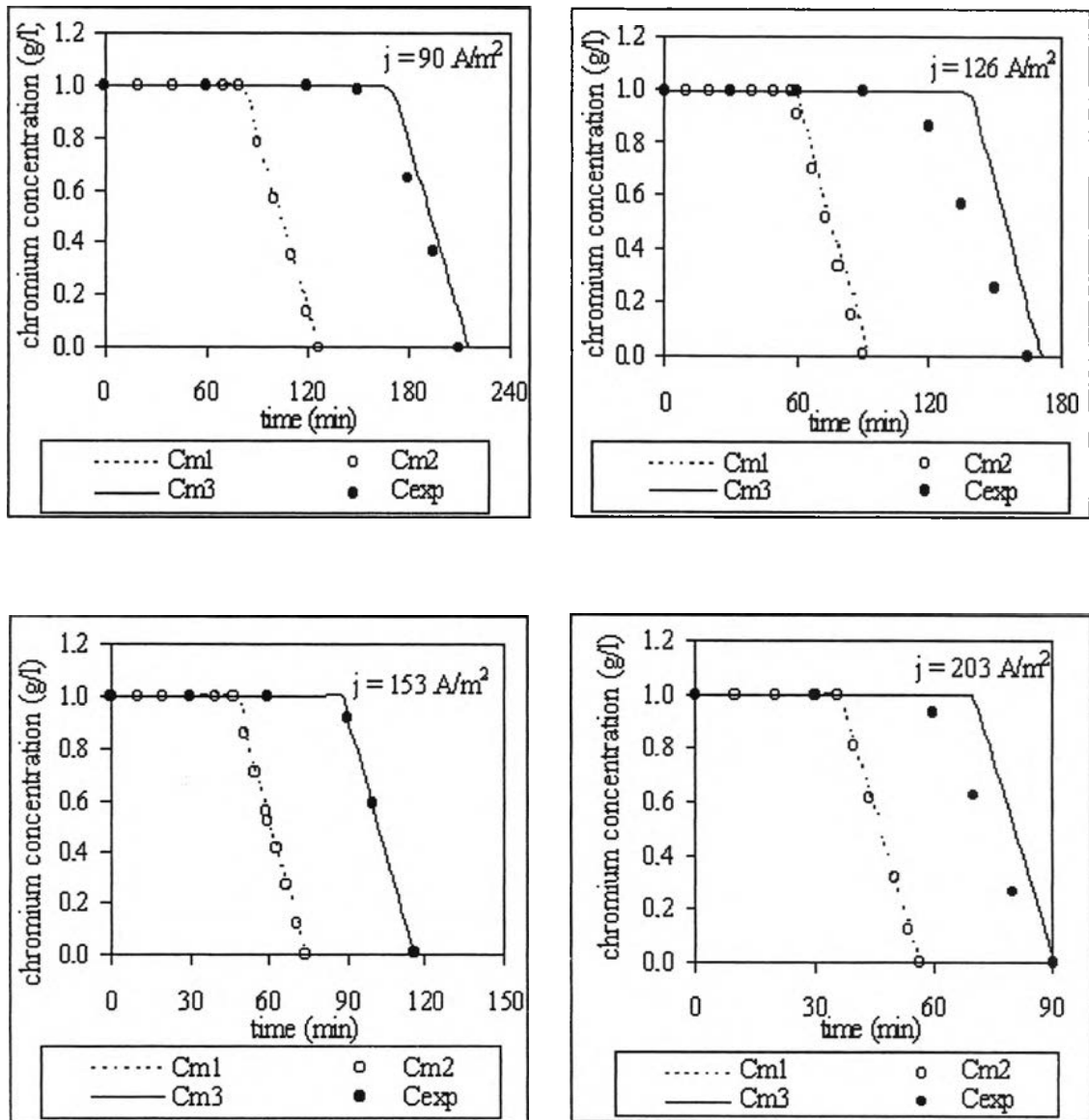


Figure V.14: Plots of C_{m1} , C_{m2} , C_{m3} and C_{exp} evolution versus time (solution S4).

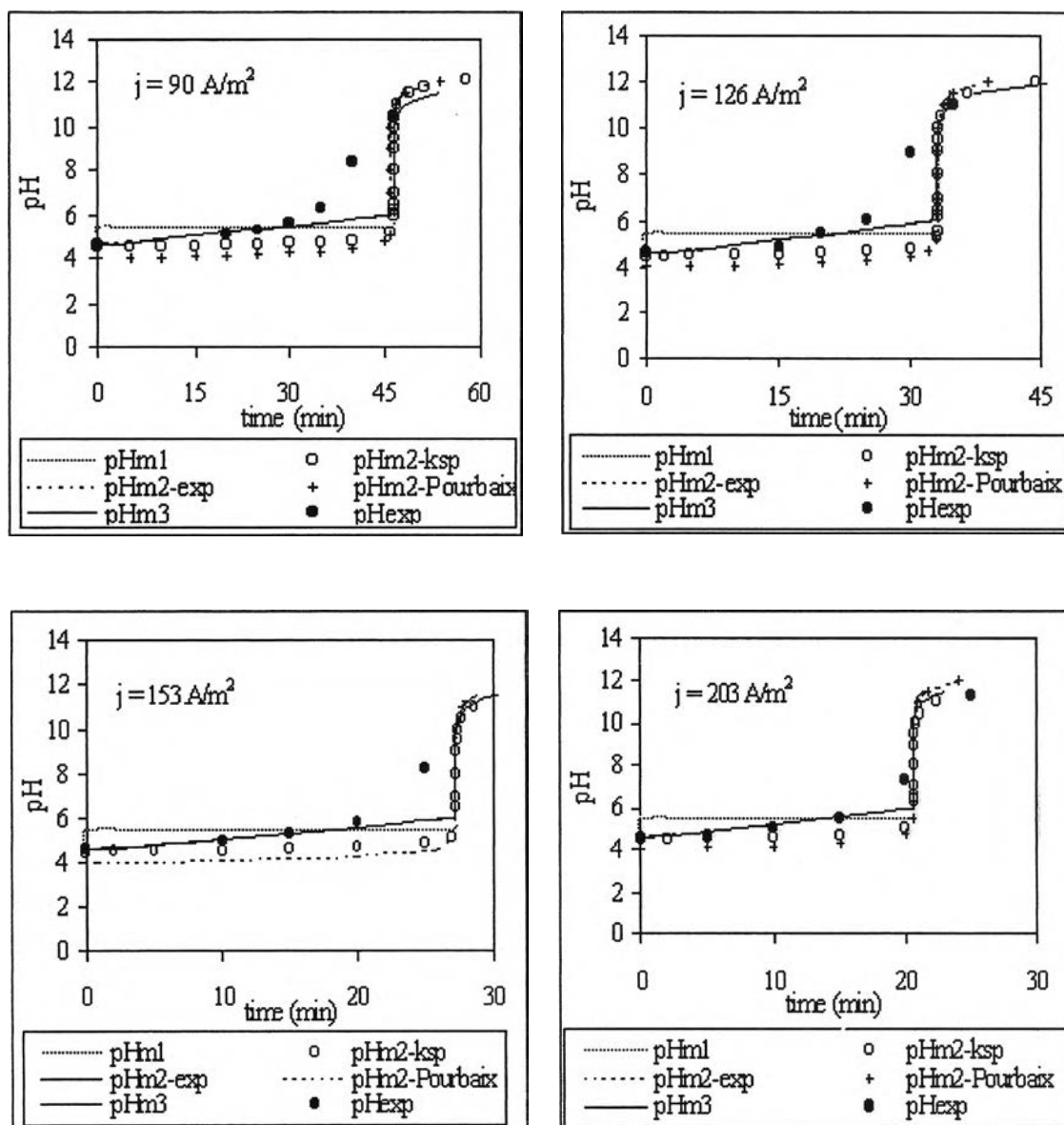


Figure V.15: Plots of pH_{m1} , pH_{m2} , pH_{m3} and pH_{exp} evolution versus time(solution S5).

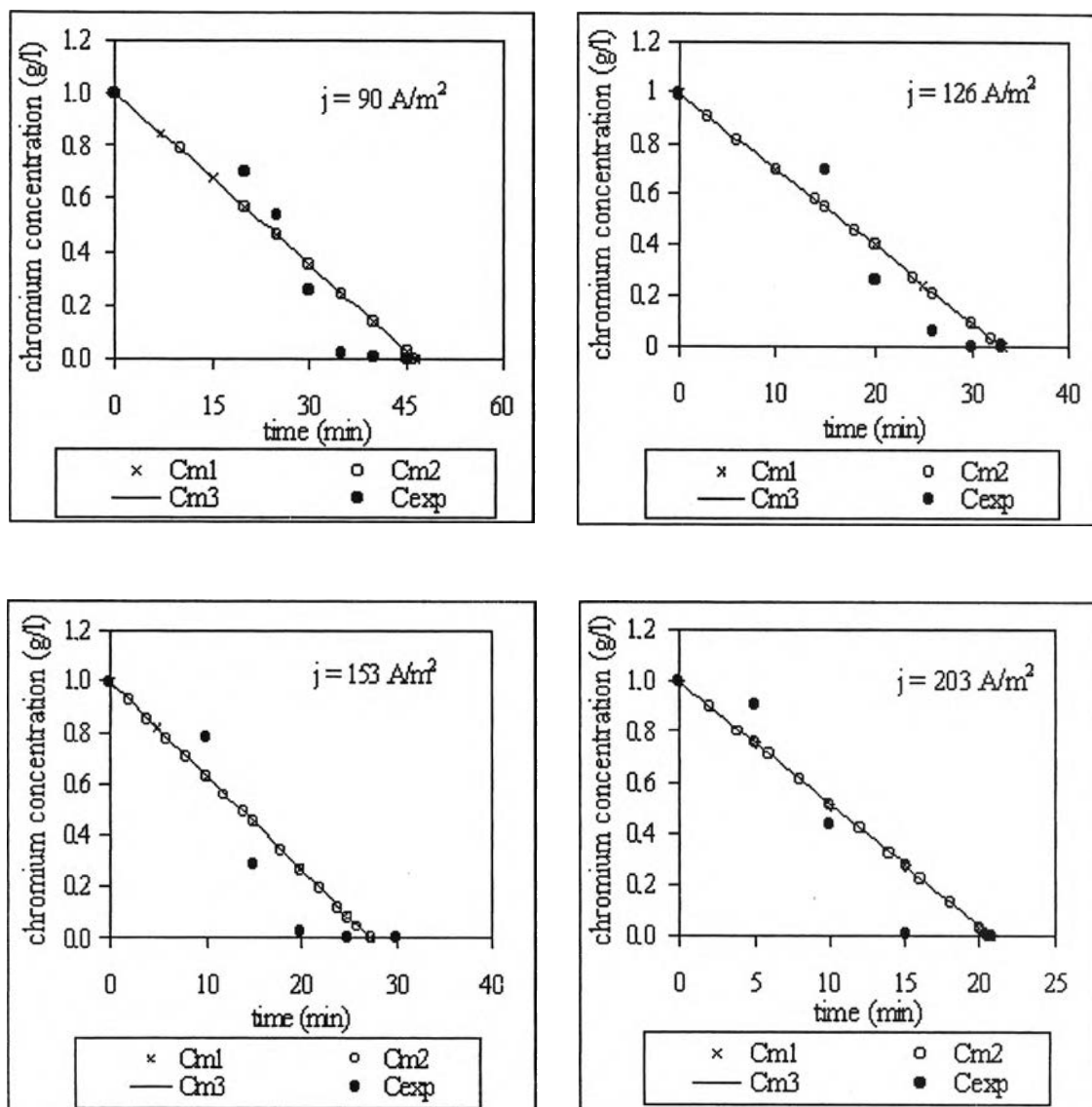


Figure V.16: Plots of C_{m1} , C_{m2} , C_{m3} and C_{exp} evolution versus time (solution S5).

For high chromium concentration, the experiment was carried out with solution S6 (10 g/l, pH = 1) and solution S7 (10 g/l, pH = 4.6) at current of 203 A/m^2 . Figure V.17 shows the experimental and the model pH (pH_{m1} , pH_{m2} and pH_{m3}) evolution. At low initial pH solution, the good fitting between experimental and calculated pH evolution was obtained by using the third model calculating with the loss flux of hydroxide ion from anodic compartment. For high initial pH solution, all model can be used to predict the pH evolution. It indicates that the precipitation process is sensitive with initial pH solution. Low initial pH solution has the large amount of proton loss from cathodic compartment to anodic compartment whereas

high initial pH solution has little amount of proton loss. This is because the latent time of low initial pH solution is longer than that of high initial pH solution.

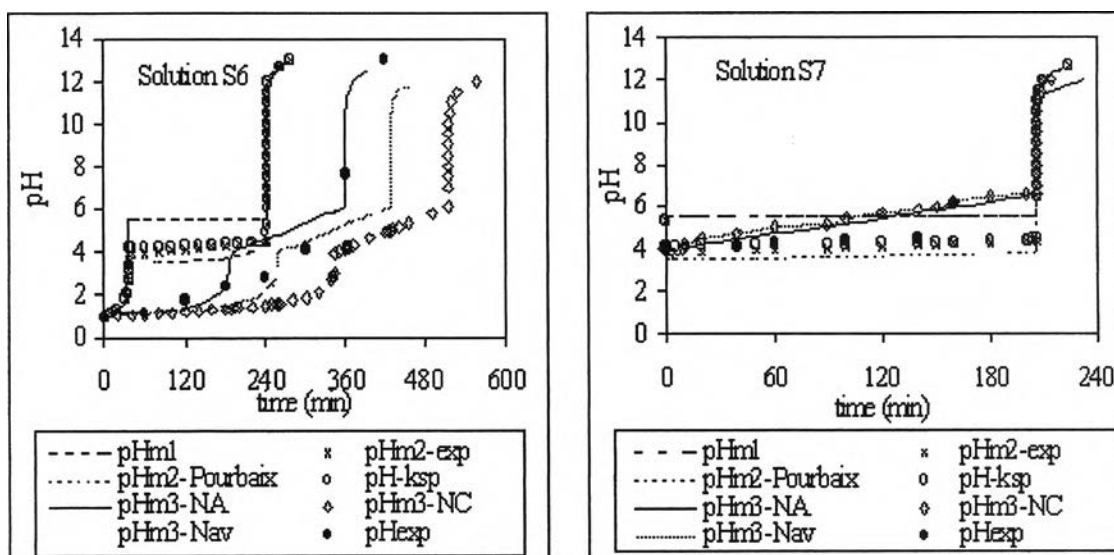


Figure V.17: Plots of pH_{m1} , pH_{m2} , pH_{m3} and pH_{exp} evolution versus time at 203 A/m^2 (solutions S6 and S7).

1.3 Influence of initial pH and initial concentration

This part considers the effect of initial pH on the chromium recovery. Figure V.18 expresses chromium recovery for solutions S4 ($\text{pH} = 1$) and S5 ($\text{pH} = 4.6$) at a current density of 203 A/m^2 . Solution S5 has high initial pH, the complete electrolysis time (≈ 20 minutes) is less than solution S4 (≈ 90 minutes) about 4 times. For the low initial pH solution (S4), the rapid precipitation rate was observed after 60 minutes whereas, for high initial pH solution, the precipitation occurred immediately after starting experiment. It showed that low initial pH solutions consume high latent time than high initial pH solution.

So in actual operation, it should be noted that the precipitation process should be performed at high pH solution to reduce the operating time and operating cost.

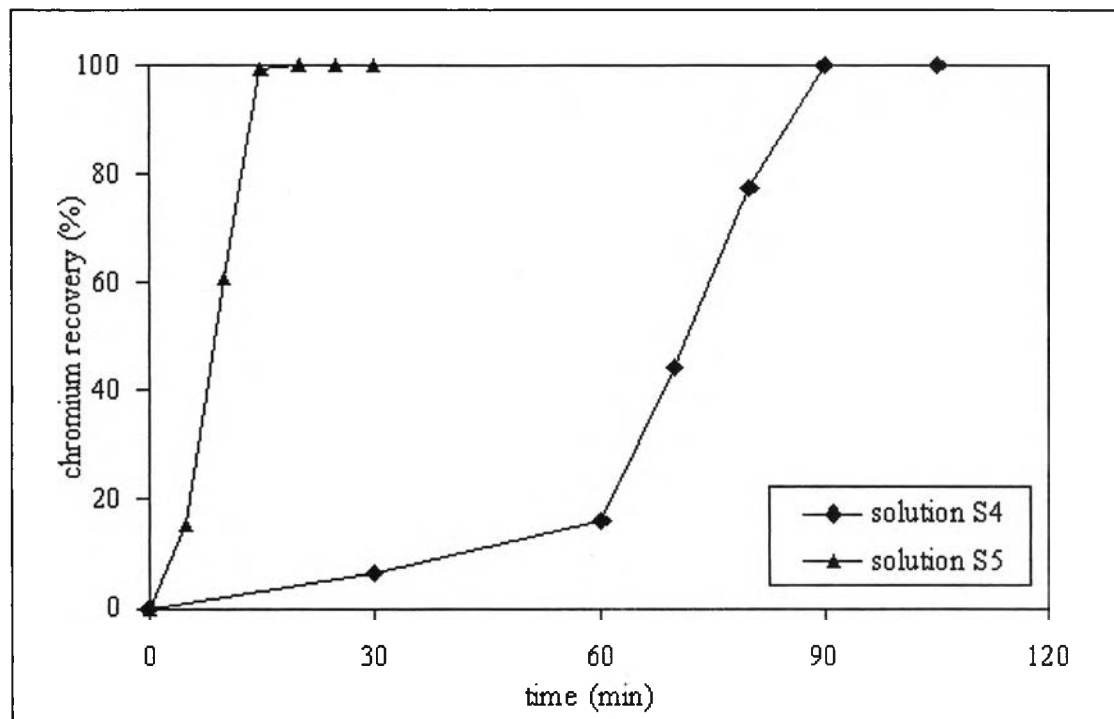


Figure V.18: Effect of initial pH on chromium recovery at 203 A/m^2 (solutions S4 and S5).

Next, experiments were performed to investigate the effect of initial concentration. Chromium concentration changed at 10 g/l at $\text{pH} = 1$. The last two curves are the plots of chromium recovery versus electrolysis time at two different initial concentrations at the same pH. Figures V.19 and V.20 demonstrate the correlation between chromium concentration versus electrolysis time under current density of 203 A/m^2 at $\text{pH} = 1$ and $\text{pH} = 4.6$, respectively. Figure V.19 shows a complete electrolysis time at lower initial concentration (solution S4) was less than 2 hours, whereas it took 6 hours at higher initial concentration (solution S6). Figure V.20 shows the same result for solution $\text{pH} = 4.6$. High initial chromium concentration (solution S7) spent about 3 hours for complete precipitation while low initial concentration (solution S5) consumed about 20 minutes at 203 A/m^2 current density which corresponds to 9 times difference. High initial concentrations have large amount of chromium ion in solution then they needed a large amount of hydroxide ion for precipitation so longer electrolysis time is observed.

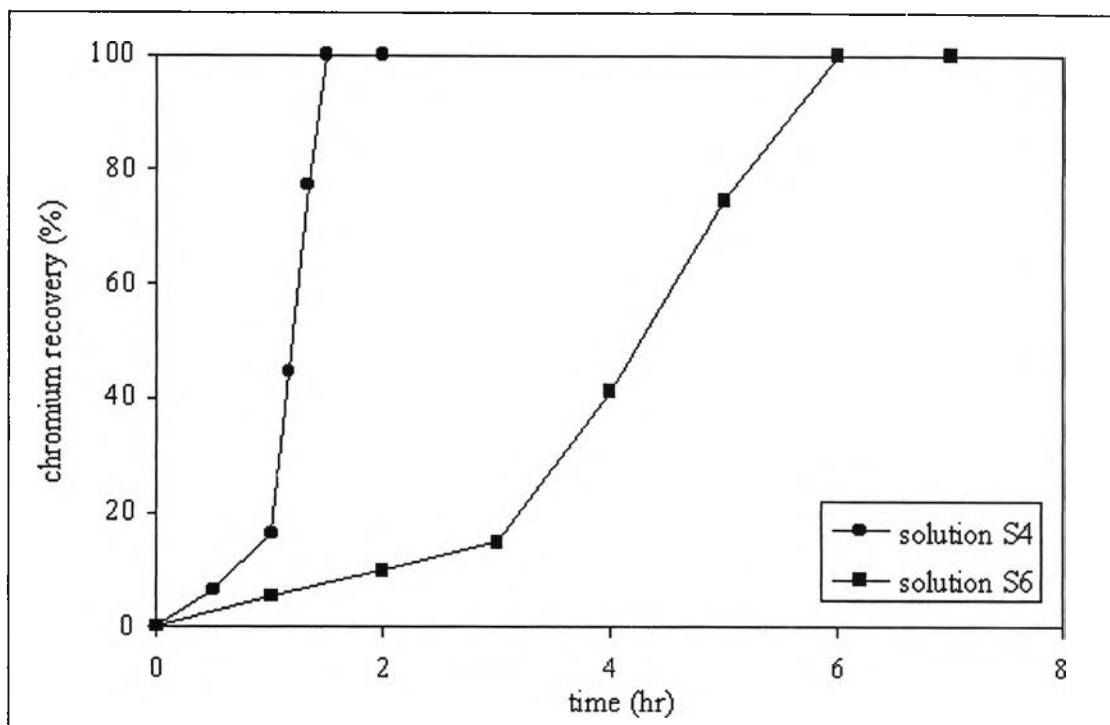


Figure V.19: Chromium recovery percentage versus time at 203 A/m^2 (solutions S4 and S6).

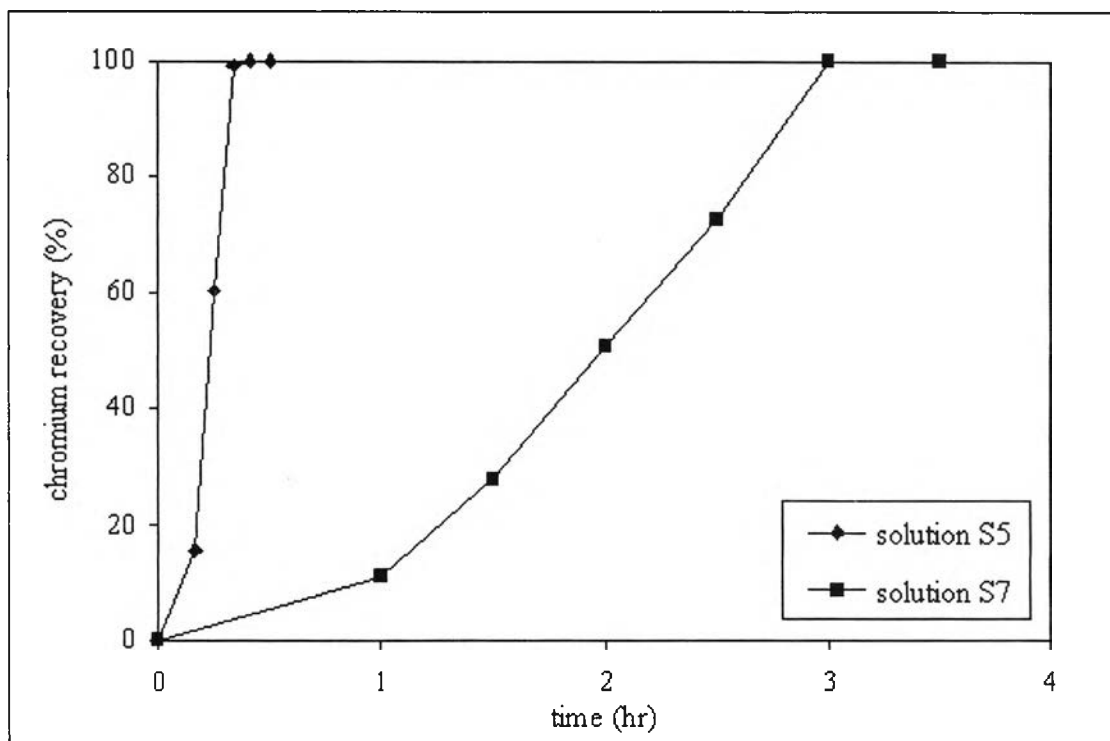


Figure V.20: Chromium recovery percentage versus time at 203 A/m^2 (solutions S5 and S7).

2. Nickel Recovery

Nickel can be recovered by electrodeposition technique but it uses a long operating time and gives very low current efficiency. Pruksathorn et al [63, 64] demonstrated that nickel with concentration of 200 mg/l at $\text{pH} \approx 2$ was recovered with current efficiency of 3.5 % at 240 A/m^2 current density. By this reason, another technique is applied to recover nickel from synthetic solution in order to get the higher current efficiency and shorter operating time. The precipitation technique seems to be a possible technique to recover nickel from a synthetic solution. A reactor with membrane as shown in Chapter III (Figure III.5) was used in this study similar to chromium recovery. The reactor was separated into two compartments by anionic membrane. The electrolyte was passing through the reactor by a pumping system and its flow rate was kept constant at around 0.42 l/min.

2.1 Influence of current density

Experiments were performed with synthetic solution of nickel at concentration of 1 g/l, $\text{pH} = 1$ (solution S8), and 1 g/l, $\text{pH} = 5$ (solution S9). H_2SO_4 and NaOH were used to adjust pH of solution to the preferable value and Na_2SO_4 was used to keep constant conductivity in range from 20 to 40 mS/cm. The current density was varied from 90 to 203 A/m^2 to detect the effect of current density on precipitation process. The amount of nickel recovery from solution S8 and solution S9 is shown respectively in Figures V.21 and V.22.

The results showed that, for the both pH solutions, nickel solutions were completely recovered at every current densities. An electrolysis time is an inverse function with current density. High applied current density led to a short operating time, whereas low applied current density granted a long operating time. Because high current density conducts high amount of electrons to the system, the large quantity of hydroxide ions is produced. Increasing current density around 1.31 times leads to decreasing electrolysis time about 0.77 times for both initial pH solutions.

In addition, at the same current density, the high initial pH solution gave the shorter operating time than the low initial pH solution did. Because a low amount of protons containing in high initial pH solution, fewer time needed to decrease number of protons and little increasing of hydroxide ion leads to fast precipitation.

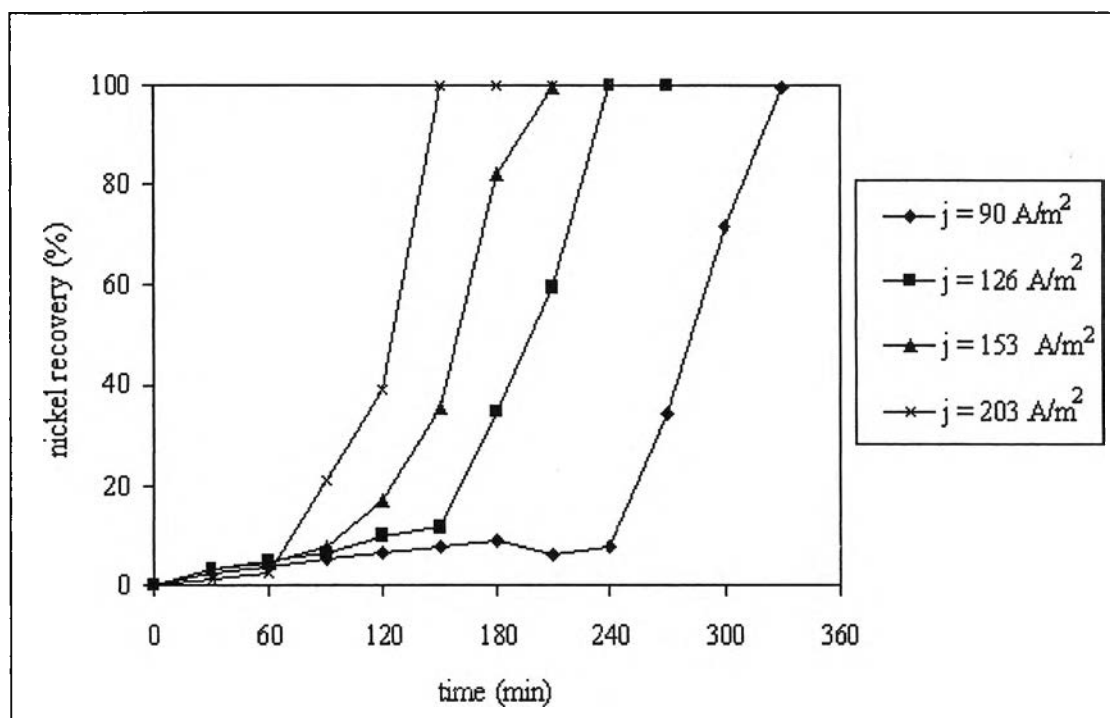


Figure V.21: Nickel recovery percentage versus time (solution S8).

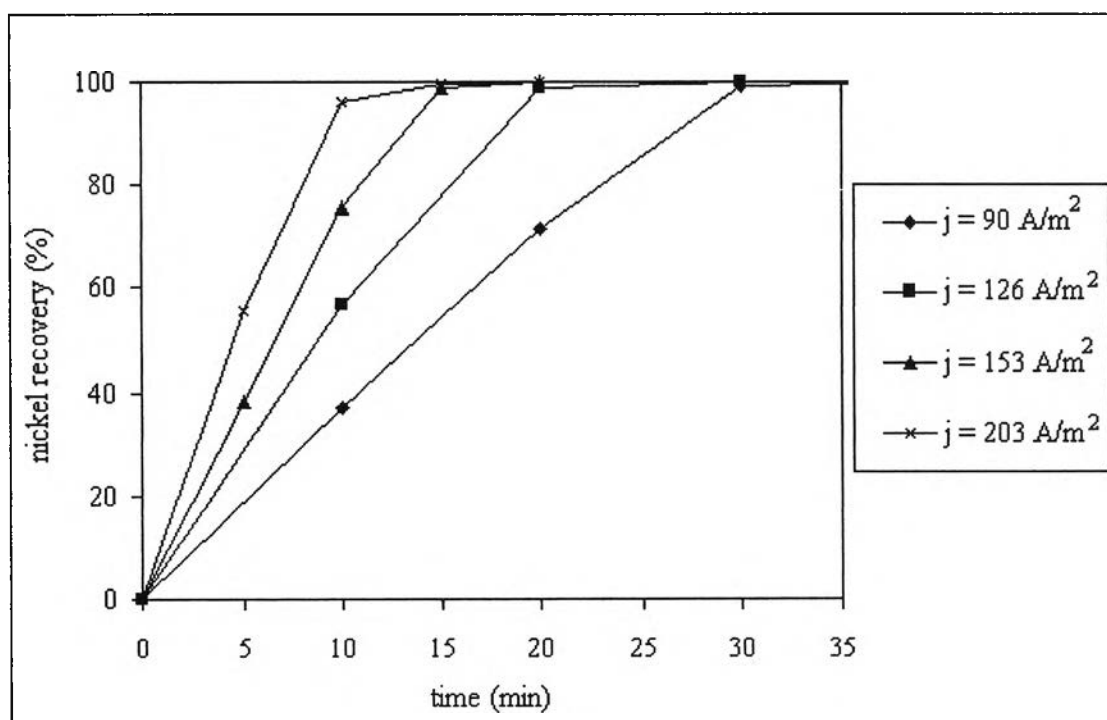


Figure V.22: Nickel recovery percentage versus time (solution S9).

The results of pH evolution in anodic, cathodic compartments and percentage of nickel recovery as a function of time (1 g/l, pH = 1 and pH = 5) are plotted respectively in Figures V.23 and V.24.

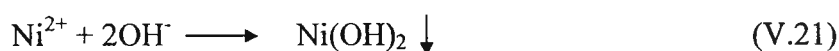
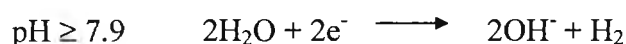
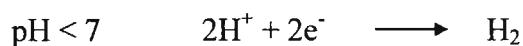
Both solutions gave the same tendency of pH evolution; ie., the pH increased in cathodic compartment but it decreased in anodic compartment. In cathodic compartment, increasing pH is caused by proton and water reduction reactions to hydrogen gas and hydroxide ions. The observed reactions in this compartment are both deposition (as white layer on cathode surface) and precipitation reactions (as green sludge). When pH is lower than precipitation pH, the deposition of nickel on electrode surface is observed during this period (equation (V.20)). The solution pH increases gradually by proton reduction (pH < 7) and water reduction (pH > 7). When pH equals to or is more than precipitation pH (pH ≈ 7.5 - 7.9), nickel ions starts to precipitate as equation(V.21) with hydroxide ions produced by the water reduction reaction. At this moment, pH of solution is constant or have a little change. Finally, after the complete precipitation, pH of solution increases rapidly because of reduction reaction of water.

On the other hand, the reaction observed in anodic compartment is oxidation reaction of water to oxygen gas and protons, so the pH in this part decreases. Following equations display reactions occurring in reactor either anodic or cathodic compartments.

Anodic compartment



Cathodic compartment



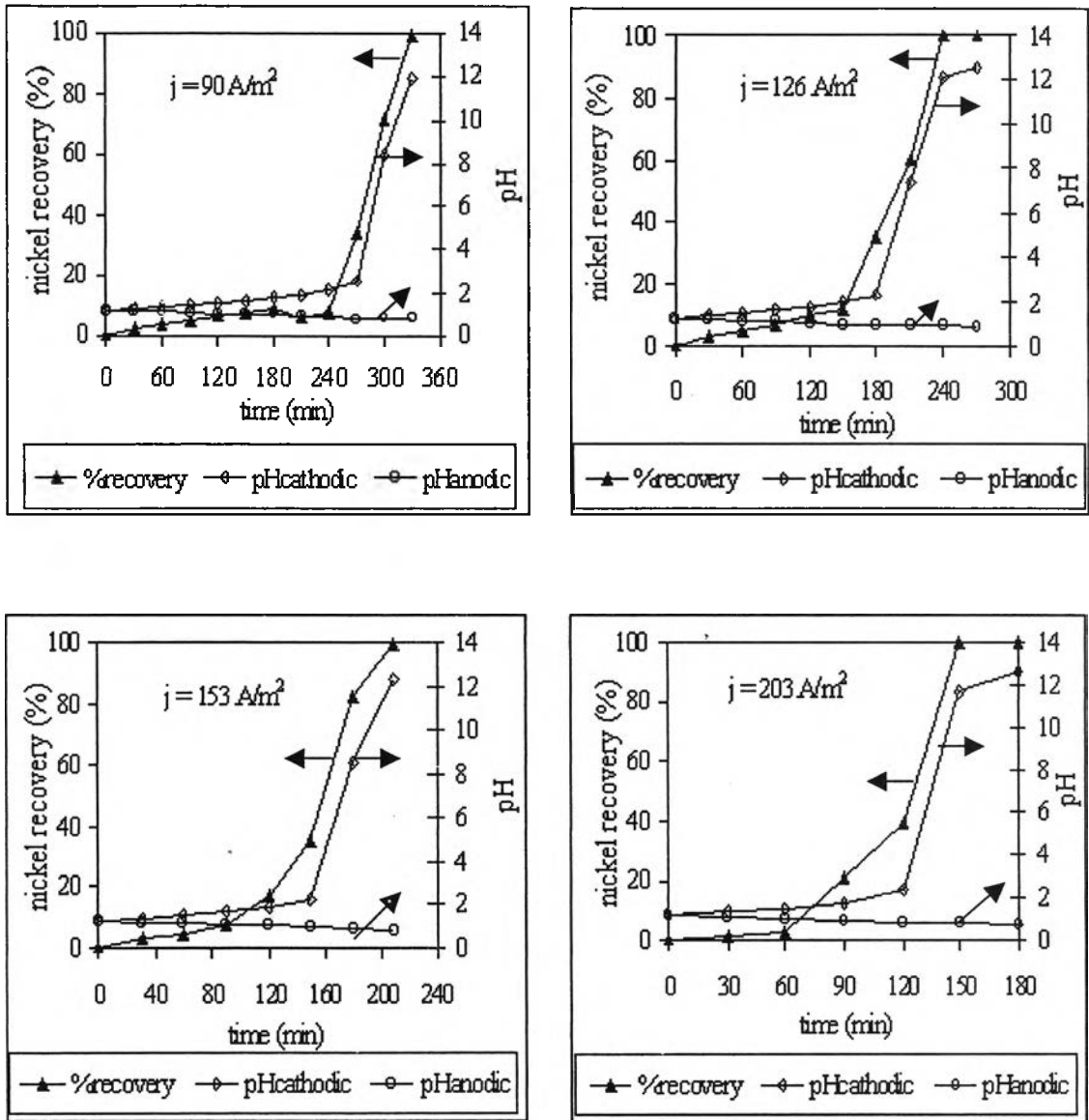


Figure V.23: Nickel recovery percentage and pH versus time (solution S8).



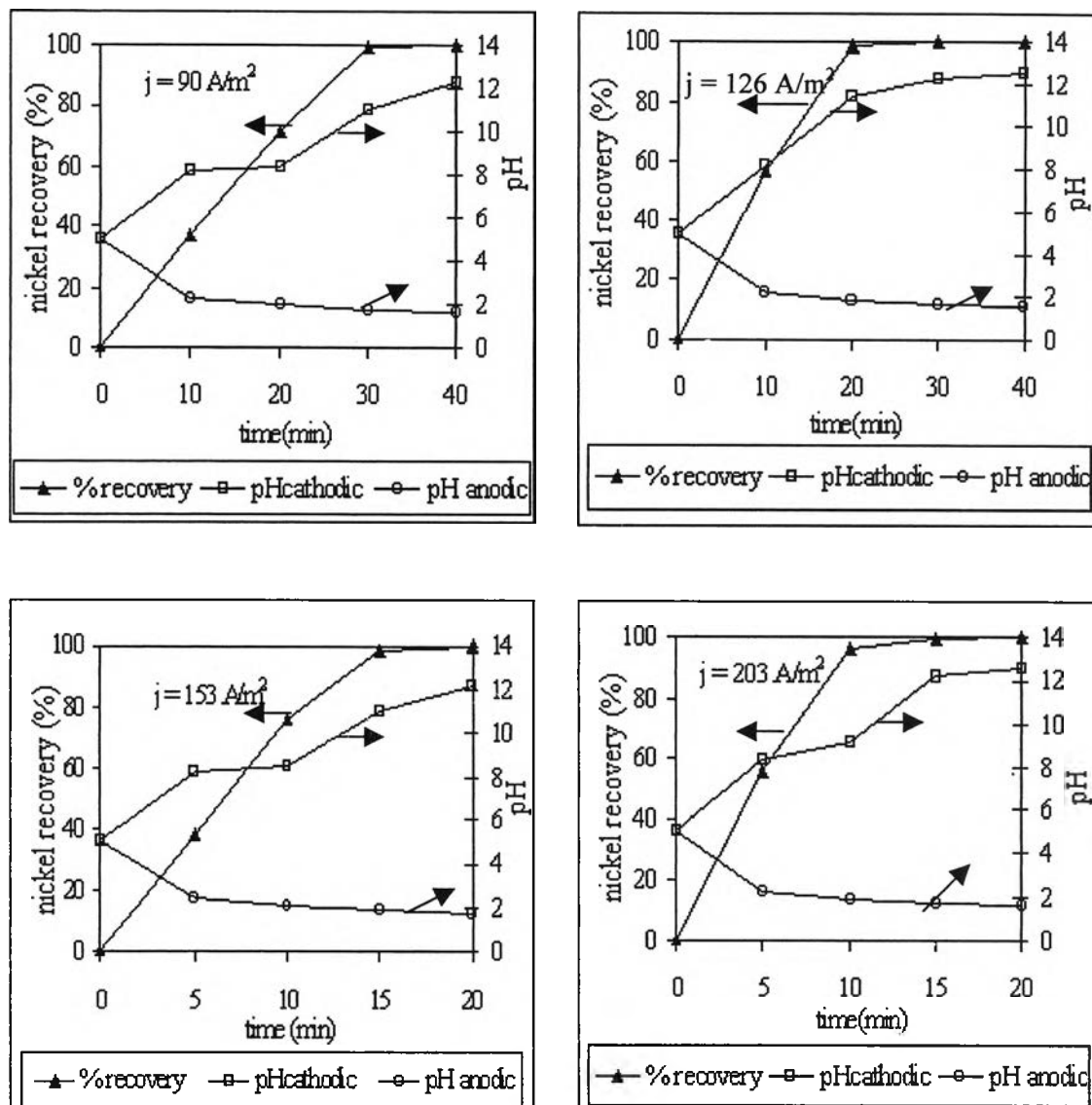


Figure V.24: Nickel recovery percentage and pH versus time (solution S9).

Figures V.25 and V.26 depict the relationship between operating cost as a function of current density of solutions S8 and S9, respectively. Operating cost which is corresponding to electricity cost is a function of applied current density and electrolysis time. The results showed that the operating cost was a direct proportion to current density. The operating cost at a range of current density from 90 to 203 A/m^2 at $\text{pH} = 1$ was between 4.42 to 8.89 $\text{US}\$/\text{m}^3$ and from 0.48 to 1.02 $\text{US}\$/\text{m}^3$ at $\text{pH} = 5$. Low initial pH solution led to approximately 9 times of operating cost higher than high initial pH solution.

Similar to chromium recovery, if experiments perform at current density less than 90 A/m^2 , the operating cost may be lower. However, the operating time will

increase which is not practical for actual operation. By this reason, experiments did not performed at current density less than 90 A/m^2 and for the continuous experiments of nickel, they will be performed at 90 A/m^2 .

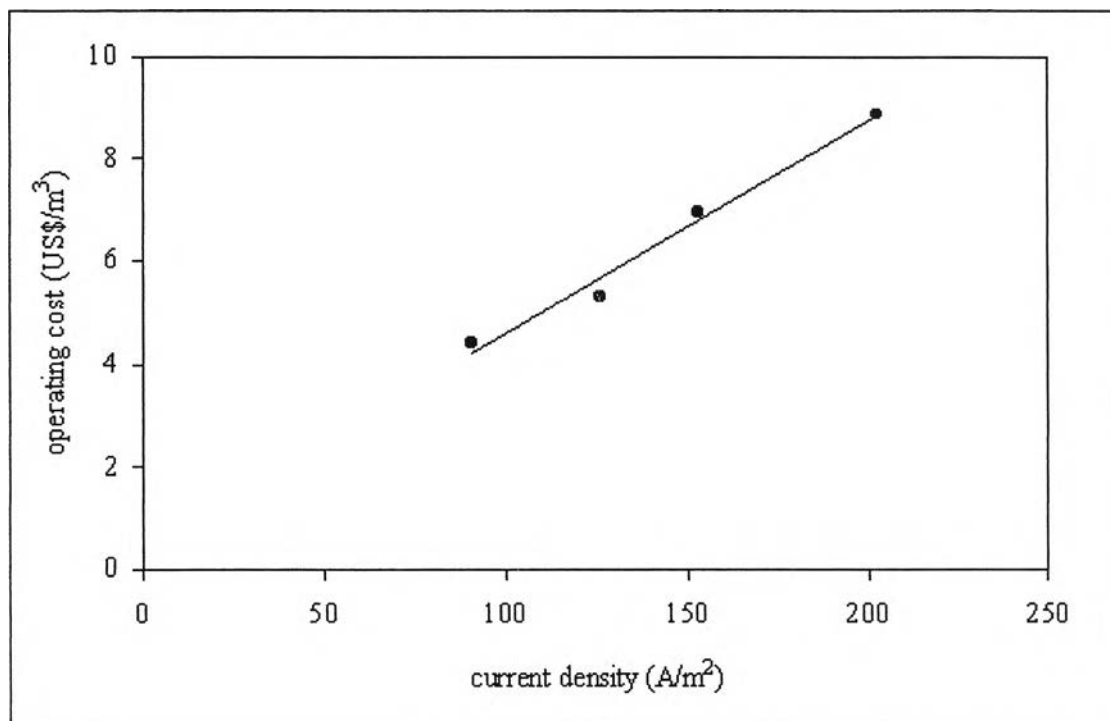


Figure V.25: Operating cost versus current density (solution S8).

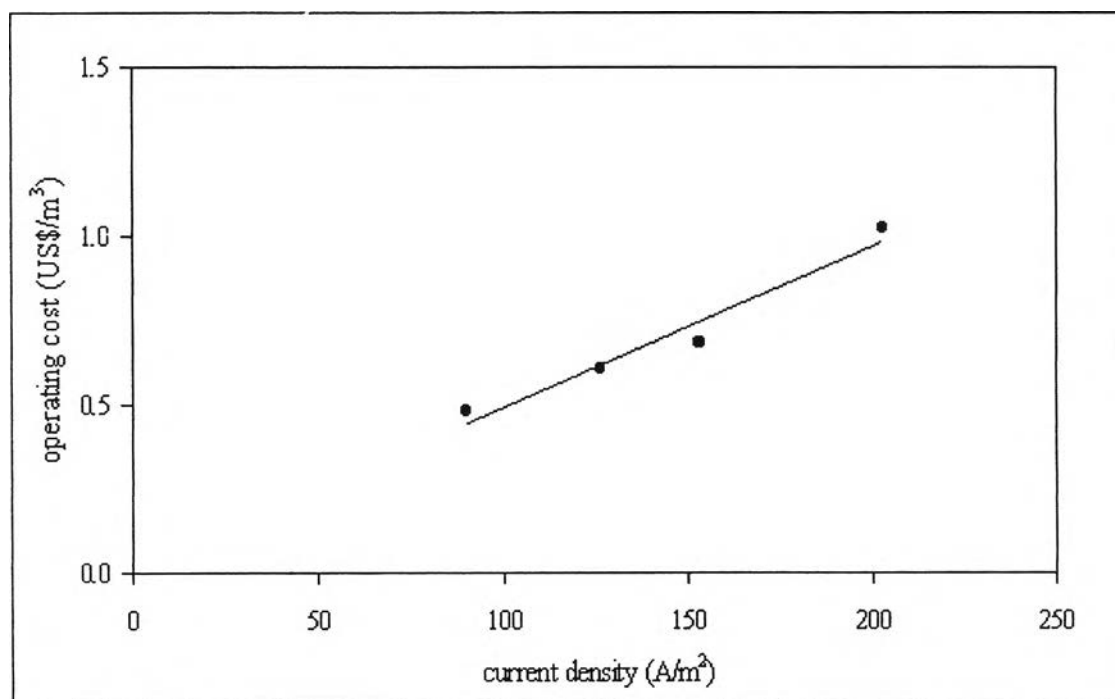


Figure V.26: Operating cost versus current density (solution S9).

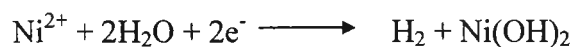
2.2 Model for nickel recovery

Three models for nickel recovery have been investigated in order to predict the pH evolution in the cathodic compartment of the reactor. The electrolysis time was separated into three zones depending on the observed reaction and pH evolution. The reactions taken place in the cathodic compartment can be described briefly by the following reactions.

1st zone



2nd zone



3rd zone



In the first zone, pH of solution increases from initial pH by reduction reaction of proton and water to hydrogen gas and hydroxide ions. At the same time, the deposition of nickel happens simultaneously. In the second zone, nickel ions in solution begin to precipitate with the hydroxide ions produced in the first zone of electrolysis time. In the last zone, after reaching the complete precipitation, the pH increases rapidly by water reduction reaction. By this process, products are both in form of pure nickel with white colour deposited on cathode surface and in form of nickel hydroxide with green colour.

2.2.1 The basic model

This model is based on two assumptions. The first is that nickel precipitates at constant pH (pH = 7.9). The second is that the loss of hydroxide ions from cathodic compartment through the membrane does not occurs. The developed model can be expressed by following equations

$$1^{st}: pH_{sol} < 7.9, [Ni^{2+}] > 0, t < t_1; t_1 = 10^{-pH_i} \frac{nFV}{i}$$

$$pH_{m1} = -\log \left[10^{-pH_i} - \left(\frac{it}{nFV} \right) \right] \quad (V.22)$$

$$2^{nd}: pH_{sol} = 7.9, [Ni^{2+}] > 0, t_1 < t < t_2; t_2 = t_1 + \frac{2nFV[Ni]}{59i}$$

$$pH_{m1} = 7.9 \quad (V.23)$$

$$3^{rd}: pH_{sol} > 7.9, [Ni^{2+}] = 0, t > t_2$$

$$pH_{m1} = -\log \left[10^{-14} \frac{nFV}{i(t-t_2)} \right] \quad (V.24)$$

In the first zone of electrolysis time, the model pH (pH_{m1}) increases from initial pH to pH about 7.9 as presented by the first zone equation. Nickel ions start to precipitate with hydroxide ions produced in the second zone of electrolysis time when pH equals to 7.9. At this period, pH remains constant at pH = 7.9. When the precipitation is completed, pH of solution rapidly increases due to water reduction reactions.

Figures V.27 and V.28 illustrate the comparison between the results obtained from the first model (pH_{m1}) and that obtained from experimental data (pH_{exp}) in the cathodic compartment at current density between 90-203 A/m². For nickel solution at pH = 1, the difference between experimental and model pH evolution was observed but for nickel solution at pH = 5, it did not. The good fitting between experimental and model pH evolution was observed by using solution at pH = 5. The difference for

low initial pH solution should come from an assumption that nickel precipitates at constant pH, so a new model with new assumptions has been developed.

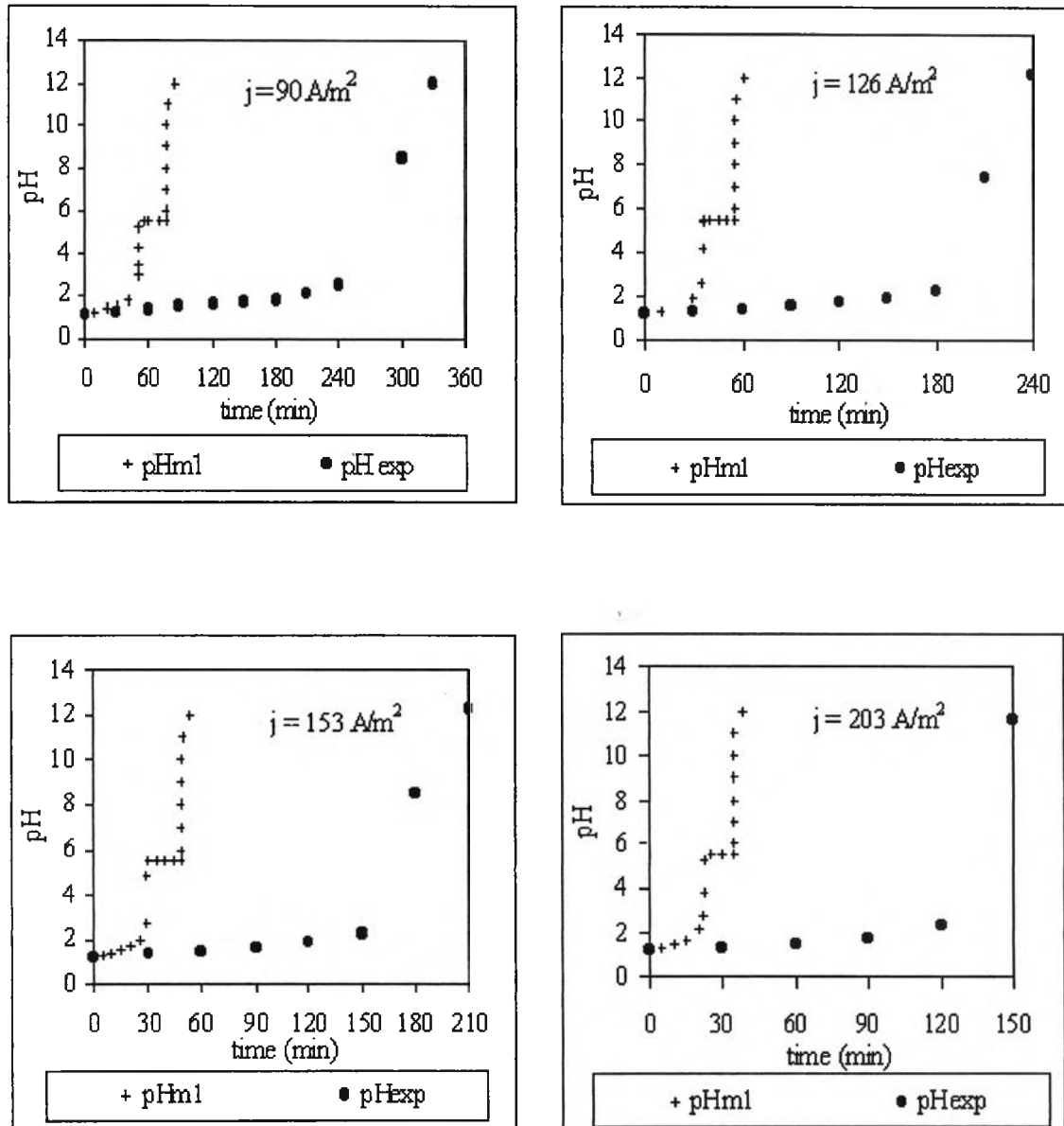


Figure V.27: Comparison between pH_{exp} and pH_{ml} evolution versus time (solution S8).

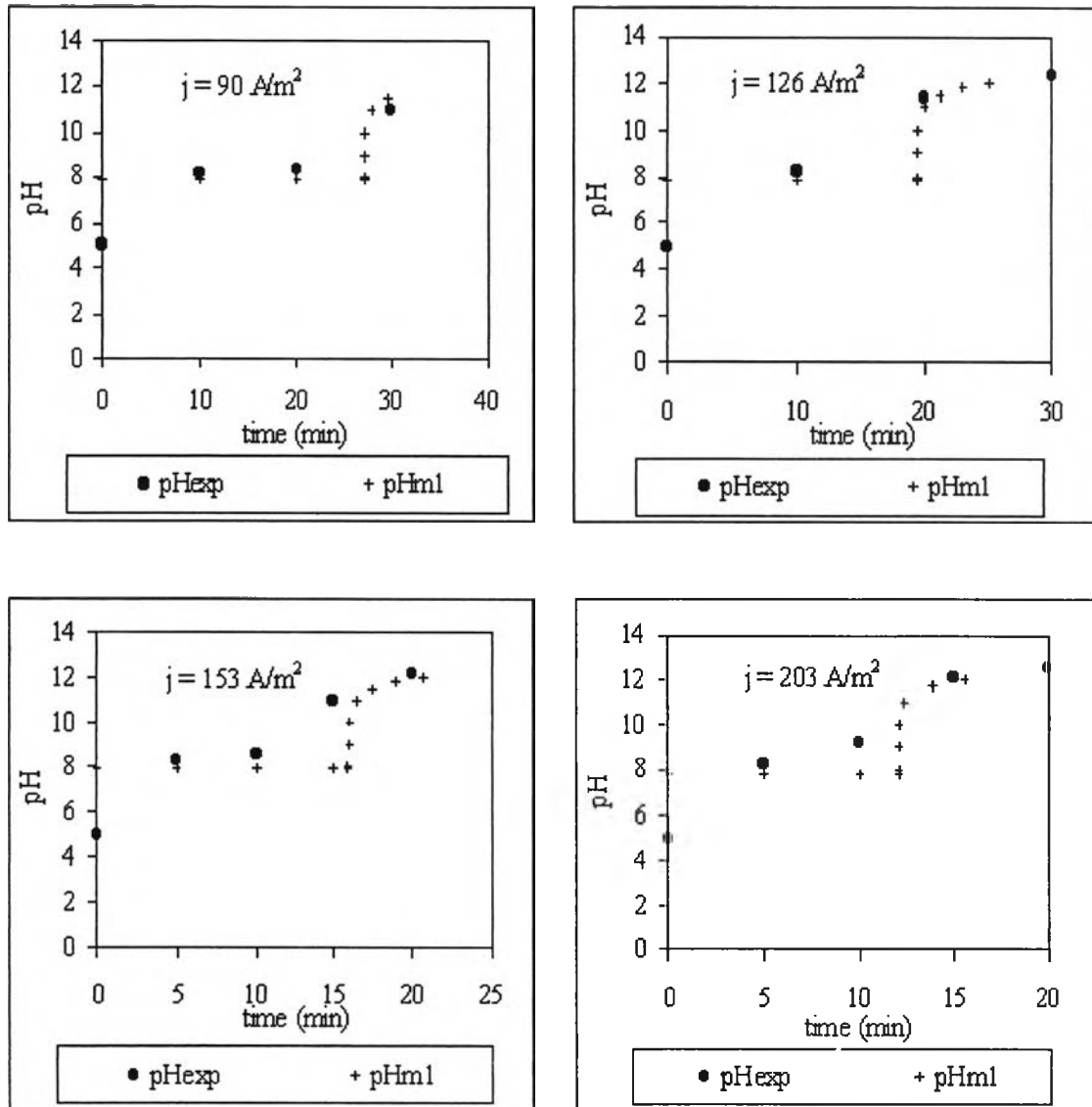


Figure V.28: Comparison between pH_{exp} and pH_{ml} evolution versus time (solution S9).

2.2.2 Non - constant pH precipitation model

The supplementary assumption of this model is that nickel precipitates at non - constant pH. In this model, the nickel precipitation data obtained from our experiment and that obtained from some references were included. The precipitation data of our experiment have been performed by adding NaOH into synthetic nickel solution. The nickel content was analysed by Atomic Absorption Spectrophotometer and, at the same time, pH of solution was collected. Figure V.29 presents the evolution between concentration versus pH value. The results showed that concentration differences were observed at the same pH.

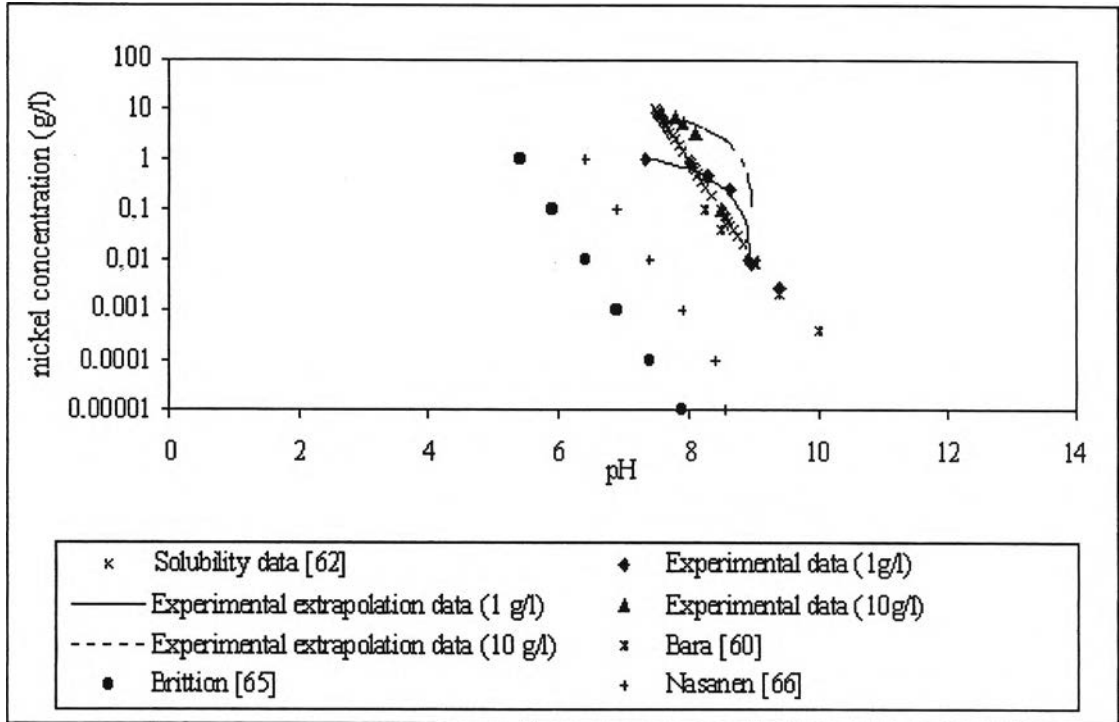


Figure V.29: Precipitation data of nickel solution.

As the previous figure, the precipitation data from our experiment and references [62, 65, 66] were included in this model and their equations were written by

$$\text{Experimental data: } pH_{\text{exp}} = \frac{[Ni] - 5.74}{-0.64} \quad (\text{V.25})$$

$$\text{Nasanen data: } pH_{\text{Nasanen}} = 6.4 - 0.217 \ln[Ni] \quad (\text{V.26})$$

$$\text{Britton data: } pH_{\text{Britton}} = 5.4 - 0.217 \ln[Ni] \quad (\text{V.27})$$

$$\text{Solubility data: } pH_{k_{sp}} = -\log k_w \left(\frac{[Ni]}{M_w k_{sp}} \right)^{\frac{1}{2}} \quad (\text{V.28})$$

where k_w equals to 10^{-14} and k_{sp} of nickel is 2×10^{-16} .

Three zones of pH evolution versus electrolysis time were used similar to the first model depending upon the observed reactions. For the first and the third zone, the model equations were exactly the same as those in the first model equations. The difference was observed in the second zone. This zone is corresponding to the precipitation zone and the precipitation data were included. The model equations followed the second model assumption can be expressed by

$$1^{st}: [Ni^{2+}] > 0, t < t_1; t_1 = 10^{-pH_1} \frac{nFV}{i}$$

$$pH_{m2} = -\log \left[10^{-pH_1} - \left(\frac{it}{nFV} \right) \right] \quad (V.29)$$

$$2^{nd}: [Ni^{2+}] > 0, t_1 < t < t_2; t_2 = t_1 + \frac{2nFV[Ni]}{59i}$$

$$pH_{m2-exp} = \left[5.74 + \frac{59i(t-t_1)}{2nFV} - [Ni] \right] / 0.64 \quad (V.30)$$

$$pH_{m2-Nasanen} = 6.4 - 0.217 \ln \left[[Ni] - \frac{59i(t-t_1)}{2nFV} \right] \quad (V.31)$$

$$pH_{m2-Britton} = 5.4 - 0.217 \ln \left[[Ni] - \frac{59i(t-t_1)}{2nFV} \right] \quad (V.32)$$

$$pH_{m2-k_{sp}} = -\log k_w \left[\frac{\left([Ni] - \frac{59i(t-t_1)}{2nFV} \right)^{1/2}}{59 k_{sp}} \right] \quad (V.33)$$

$$3^{rd}: [Ni^{2+}] = 0, t > t_2$$

$$pH_{m2} = -\log \left[10^{-14} \frac{nFV}{i(t-t_2)} \right] \quad (V.34)$$

In the cathodic compartment, pH increases as the first zone equation until electrolysis time equals to t_1 . After that, nickel ions in solution begin to precipitate as the precipitation equation used. When the complete precipitation of nickel is reached, pH of solution sharply increases as given by the third zone equation corresponding to water reduction reaction to hydrogen gas and hydroxide ions.

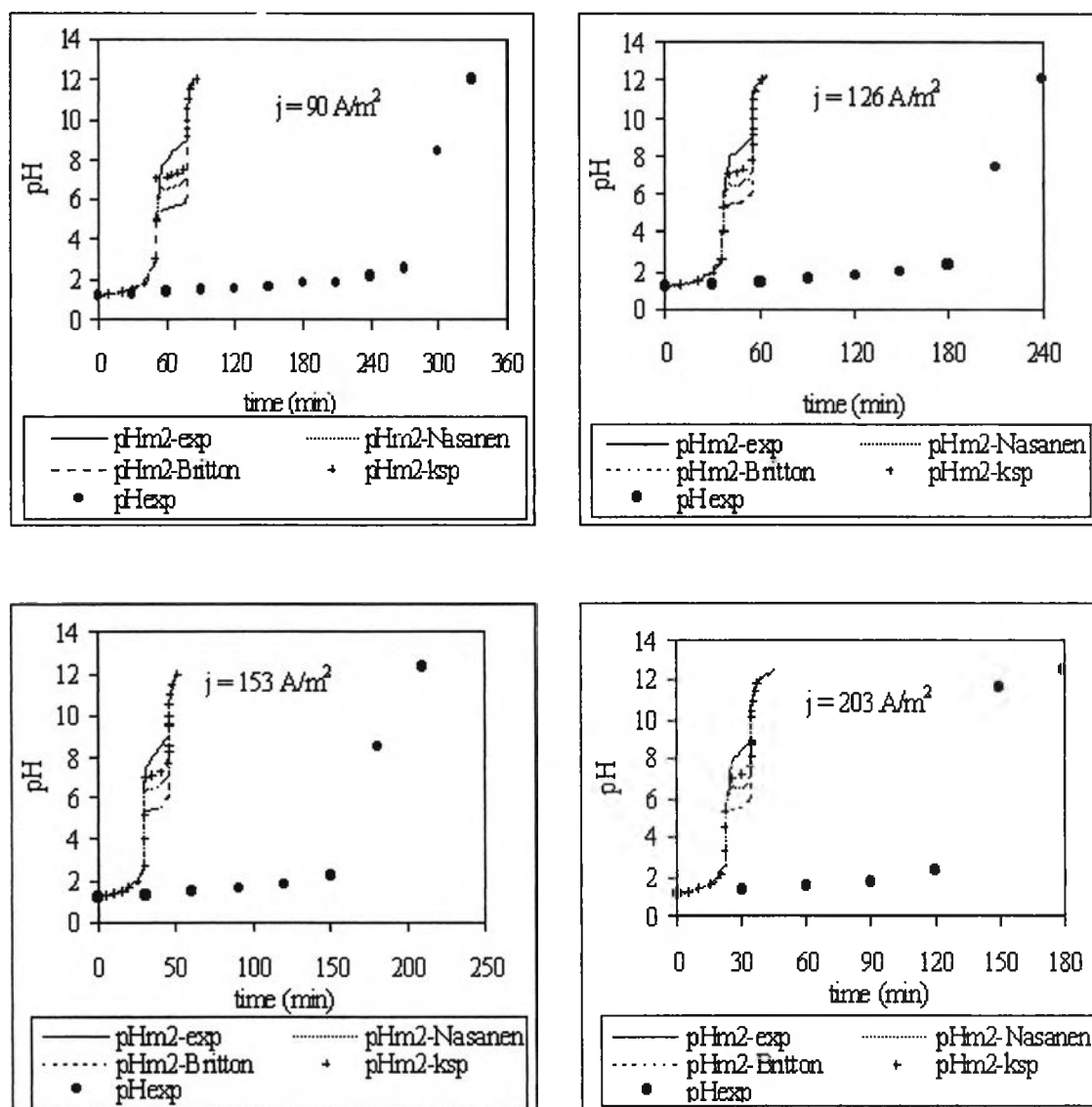


Figure V.30: Comparison between pH_{exp} and pH_{m2} evolution versus time (solution S8).

Figure V.30 presents the comparison plot between experimental and model pH versus time at current density of 90 - 203 A/m^2 for solution S8 (1 g/l, $\text{pH} = 1$). The results showed that large differences between experimental and model pH evolutions were observed. The experimental pH evolution needed electrolysis time longer than

the model pH evolution. It implies that the previous hypothesis is not sufficient to predict pH evolution in cathodic compartment and the difference between experimental and model pH do not come from precipitation equation used.

For high initial pH solution, the plot between experimental and model pH evolution of nickel with initial concentration of 1 g/l at pH = 5 (solution S9) is shown in Figure V.31. It shows that the good agreement was obtained. The electrolysis times of all models calculated by several precipitation equations were quite the same with that of experiment, and the model calculated by experimental precipitation data gave the best fitting than the other models.

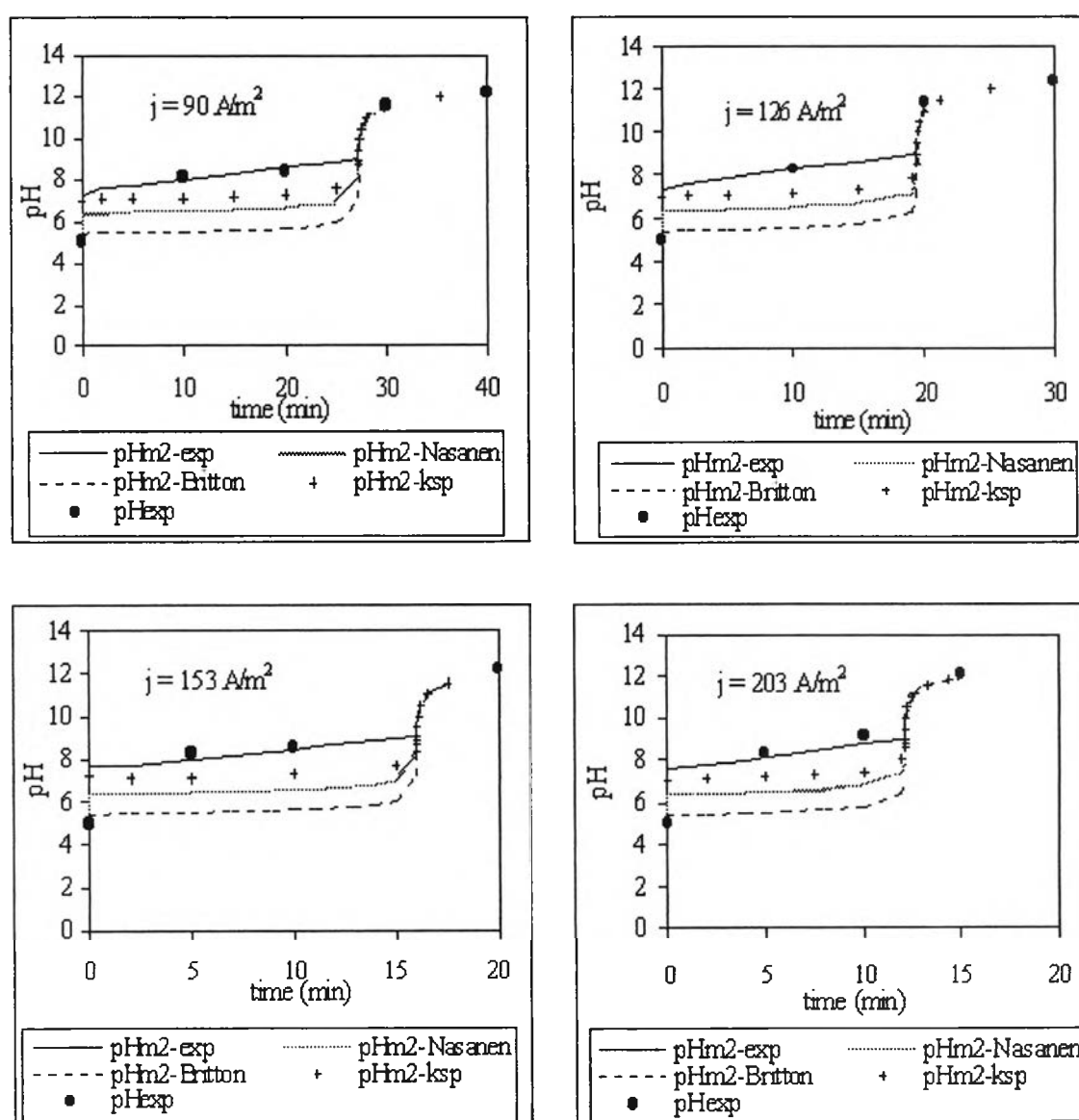


Figure V.31: Comparison between pH_{exp} and pH_{m2} evolution versus time (solution S9).

2.2.3 Non - constant pH precipitation with loss flux of hydroxide ion model

This model had a supplementary assumption that loss flux of hydroxide ions through the membrane is taken place in the system. The loss flux of hydroxide ions is normally in equilibrium with the amount of proton consumption in the reaction, so the loss flux of hydroxide ions is searched by the material balance of proton in the anodic and the cathodic compartments. The material balance of protons is shown in Appendix A.6.

Table V.2 presents the value of proton loss flux obtained from the material balance between the anodic and the cathodic compartments. The results showed the difference of proton loss flux in cathodic and anodic compartment. So, in the third model, these loss fluxes of hydroxide ions were substituted in order to determine the best adequateness with experimental results. In addition, it was assumed that the loss flux didn't presented during precipitation period because, pH in the anodic compartment decreased quickly during this period.

Table V.2: Material balance of proton in nickel precipitation process.

Current density, (A/m ²)	N _{H+} from cathodic part, (mol/m ² s)	N _{H+} from anodic part, (mol/m ² s)	N _{H+} average, (mol/m ² s)
90	1.13 x 10 ⁻³	1.07 x 10 ⁻³	1.10 x 10 ⁻³
126	1.59 x 10 ⁻³	1.50 x 10 ⁻³	1.55 x 10 ⁻³
153	1.95 x 10 ⁻³	1.84 x 10 ⁻³	1.90 x 10 ⁻³
203	2.69 x 10 ⁻³	2.40 x 10 ⁻³	2.55 x 10 ⁻³

pH evolution was classified into three zones. The first and the third zones of this model were similar to those of two previous models while the equation calculated by experimental data was included in the second zone.

The equations for this model can be written by the following

$$1^{st}: [Ni^{2+}] > 0, t < t_1; t_1 = \frac{10^{-pH_1}}{\left[\frac{i}{nFV} - \frac{N_{H^+}A}{V} \right]}$$

$$pH_{m3} = -\log \left[10^{-pH_1} - \left(\frac{it}{nFV} \right) + \frac{N_{H^+}At}{V} \right] \quad (V.35)$$

$$2^{nd}: [Ni^{2+}] > 0, t_1 < t < t_2; t_2 = t_1 + \frac{2nFV[Ni]}{59i}$$

$$pH_{m3} = \left[5.74 + \frac{59i(t-t_1)}{2nFV} - [Ni] \right] / 0.64 \quad (V.36)$$

$$3^{rd}: [Ni^{2+}] = 0, t > t_2$$

$$pH_3 = -\log \left[\frac{10^{-14}}{(t-t_2) \left[\frac{i}{nFV} - \frac{N_{H^+}A}{V} \right]} \right] \quad (V.37)$$

where A is the area of membrane.

The plots of the third model are shown in Figure V.32. It shows the same tendency as that obtained from chromium recovery. The model included loss flux of hydroxide ions calculated from anodic compartment gave the best fitting with experimental results. The reason should be that the material balance of proton in the cathodic compartment had low precision due to our assumption. Our assumption was based on only one reaction taken place at one zone. However, the reaction takes place in each zone may be more than one reaction such as water reduction or proton reduction in the first zone of electrolysis time. By this reason, the current efficiency

that we generally suppose 100 % is always less than, so the exact value of loss flux does not obtained. In the anodic compartment, on the other hand, it had only water oxidation reaction to oxygen gas and protons. The more precision of material balance in the anodic compartment than the another one is obtained.

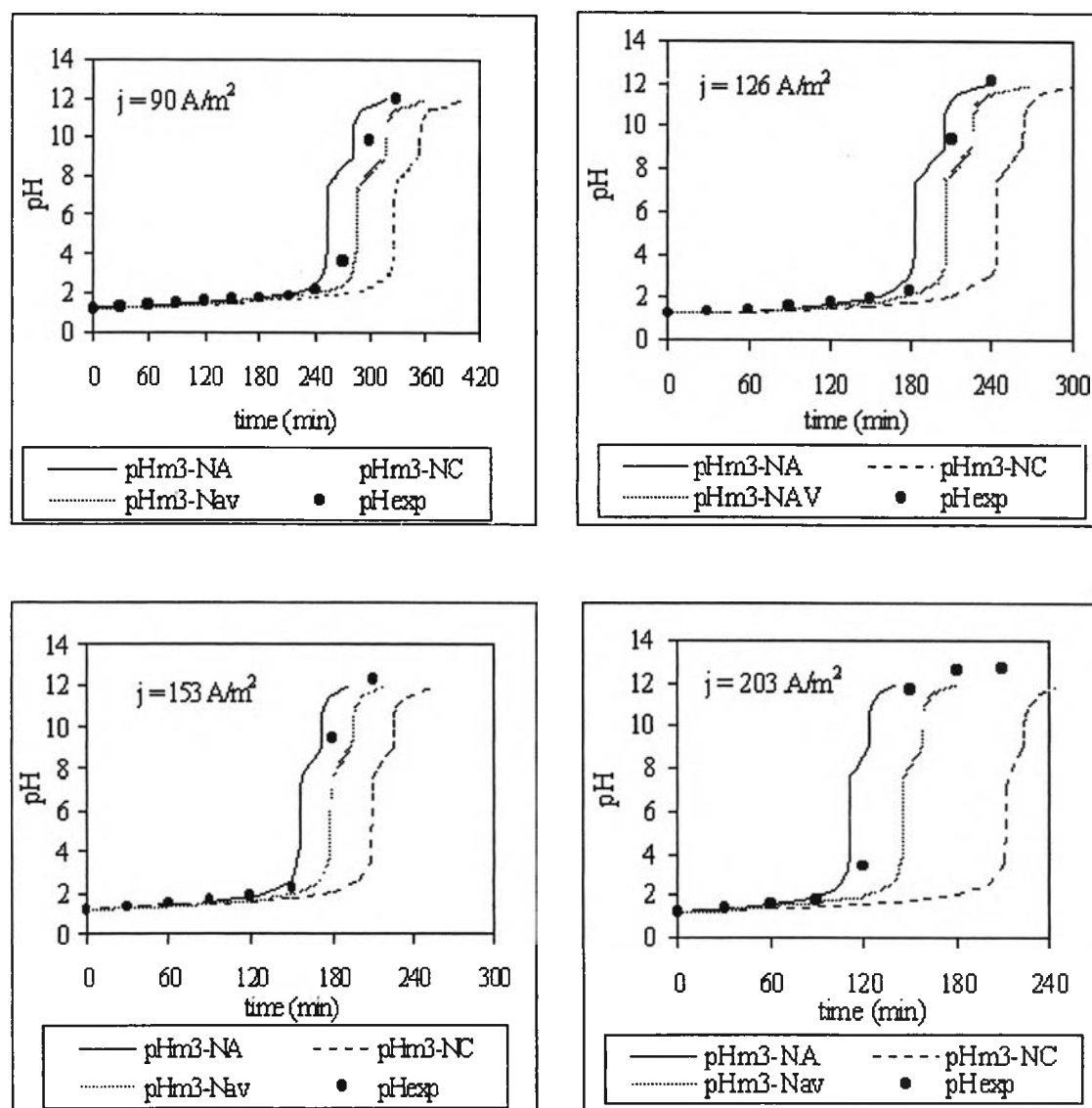


Figure V.32: Comparison between pH_{exp} and pH_{m3} evolution versus time (solution S8).

where $\text{pH}_{\text{m3-NA}}$, $\text{pH}_{\text{m3-NC}}$, $\text{pH}_{\text{m3-Nav}}$ and pH_{exp} are the pH evolution given by loss flux from anodic and cathodic compartments, an average and experiment, respectively.

Figures V.33 and V.34 show the plots of pH calculated by the first, the second, the third model and experimental results of solution S8 and S9, respectively. They show that the third model gave the best fitting with experimental results for both pH

solution. The loss flux of hydroxide ion has effect on low initial pH system because the increasing of solution pH to precipitation pH uses long electrolysis time. So the large amount of hydroxide ions is loss in cathodic compartment. On the other hand, the loss flux of hydroxide ions has no effect on high initial pH system because the solution has large amount of hydroxide ions .

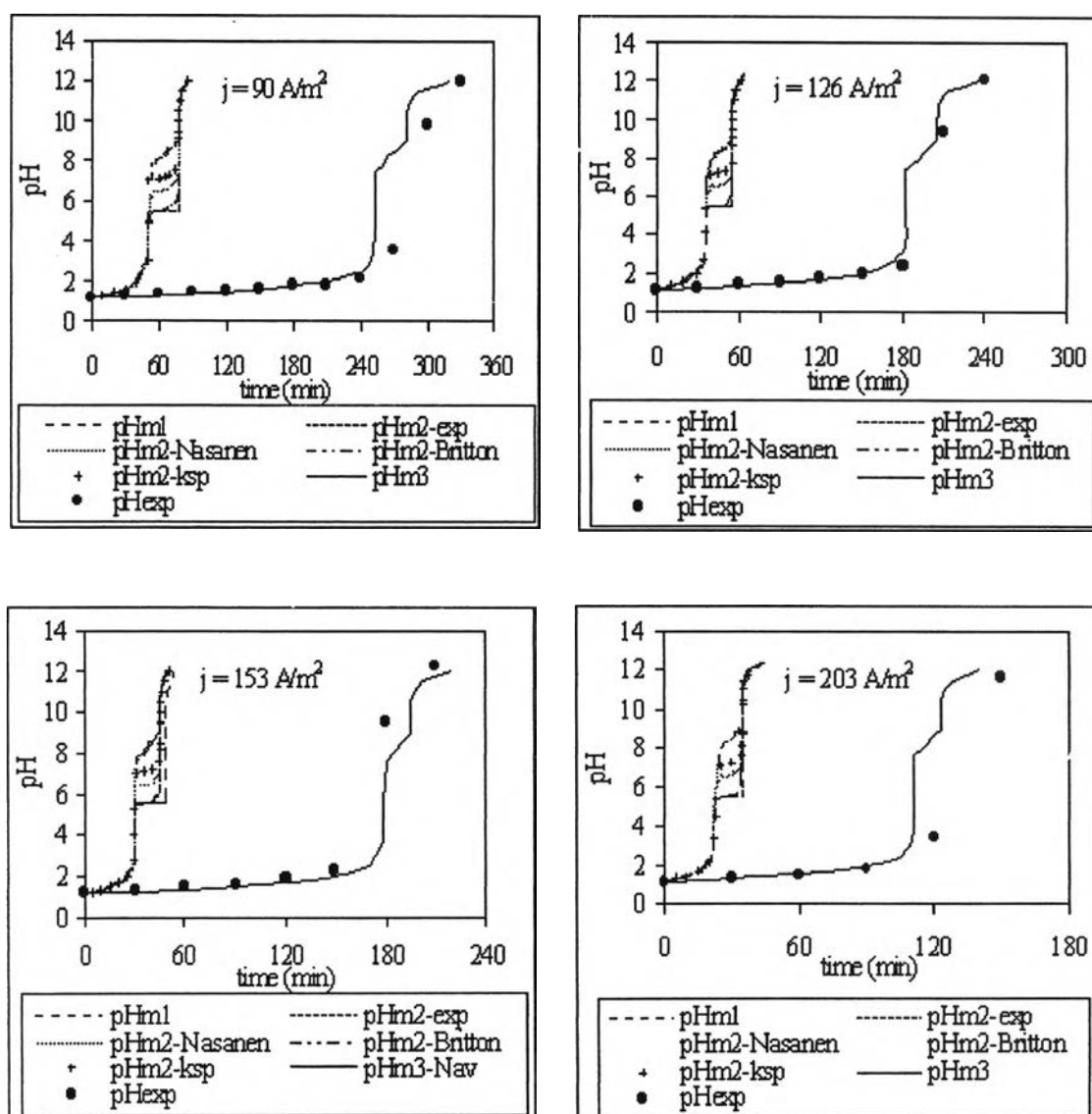


Figure V.33: Plots of pH_{m1} , pH_{m2} , pH_{m3} and pH_{exp} evolution versus time (solution S8).

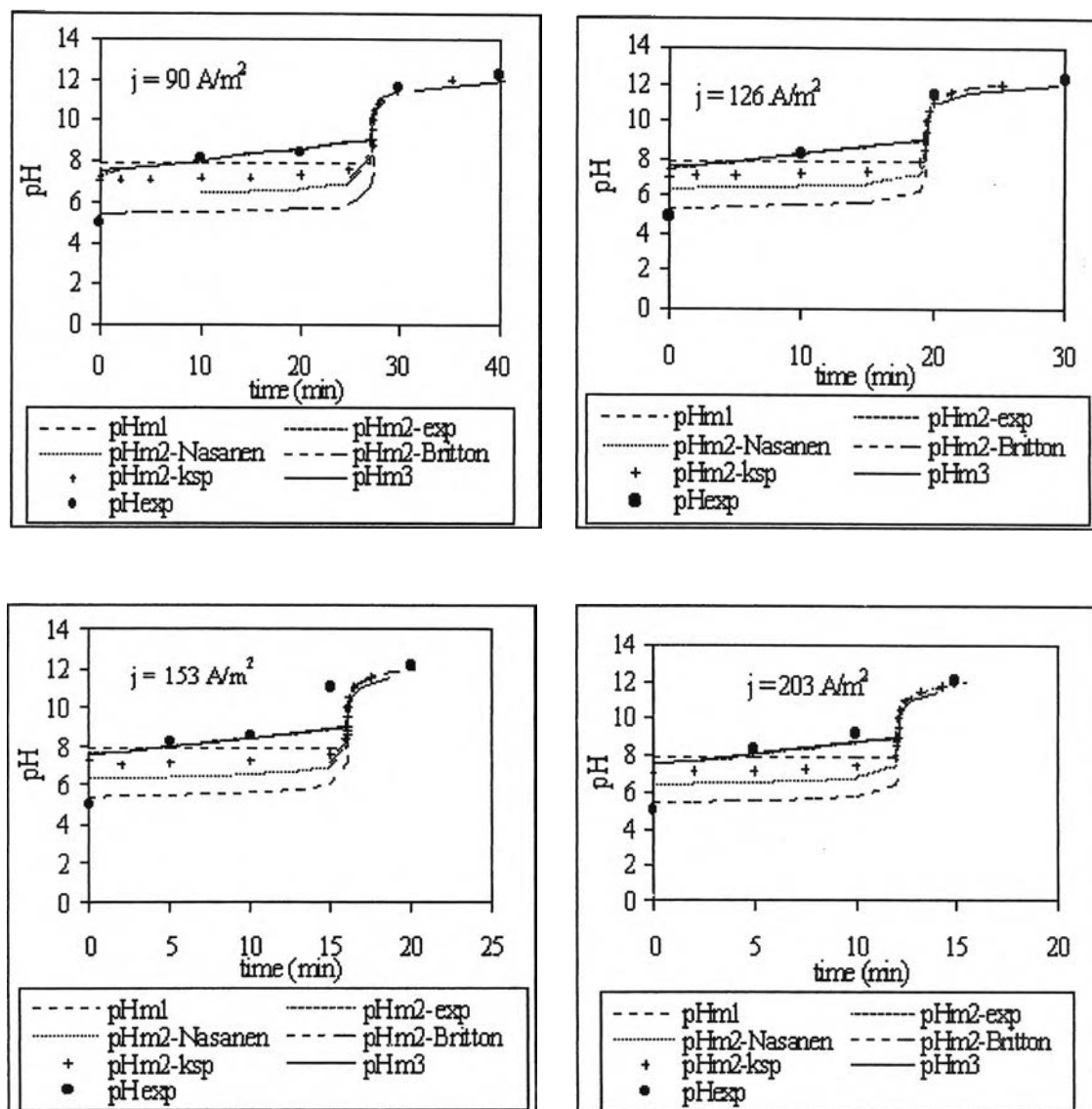


Figure V.34: Plots of pH_{m1} , pH_{m2} , pH_{m3} and pH_{exp} evolution versus time (solution S9).

The concentration evolution at all current density corresponding to the previous three models of solution S8 and S9 are plotted in Figures V.35 and V.36. By using the third model, the good fitting between experimental and calculated pH is obtained for both low and high initial pH solutions. For low initial pH solution (solution S8), a little difference between model (C_{m3}) and experimental (C_{exp}) concentration was observed because of little nickel deposition on cathode surface. When, the current density increases, the difference between those concentration increases because high applied current density conducts high nickel deposition followed the Faraday's law. For high initial pH solution (solution S9), the deposition didn't observe during the experiment.

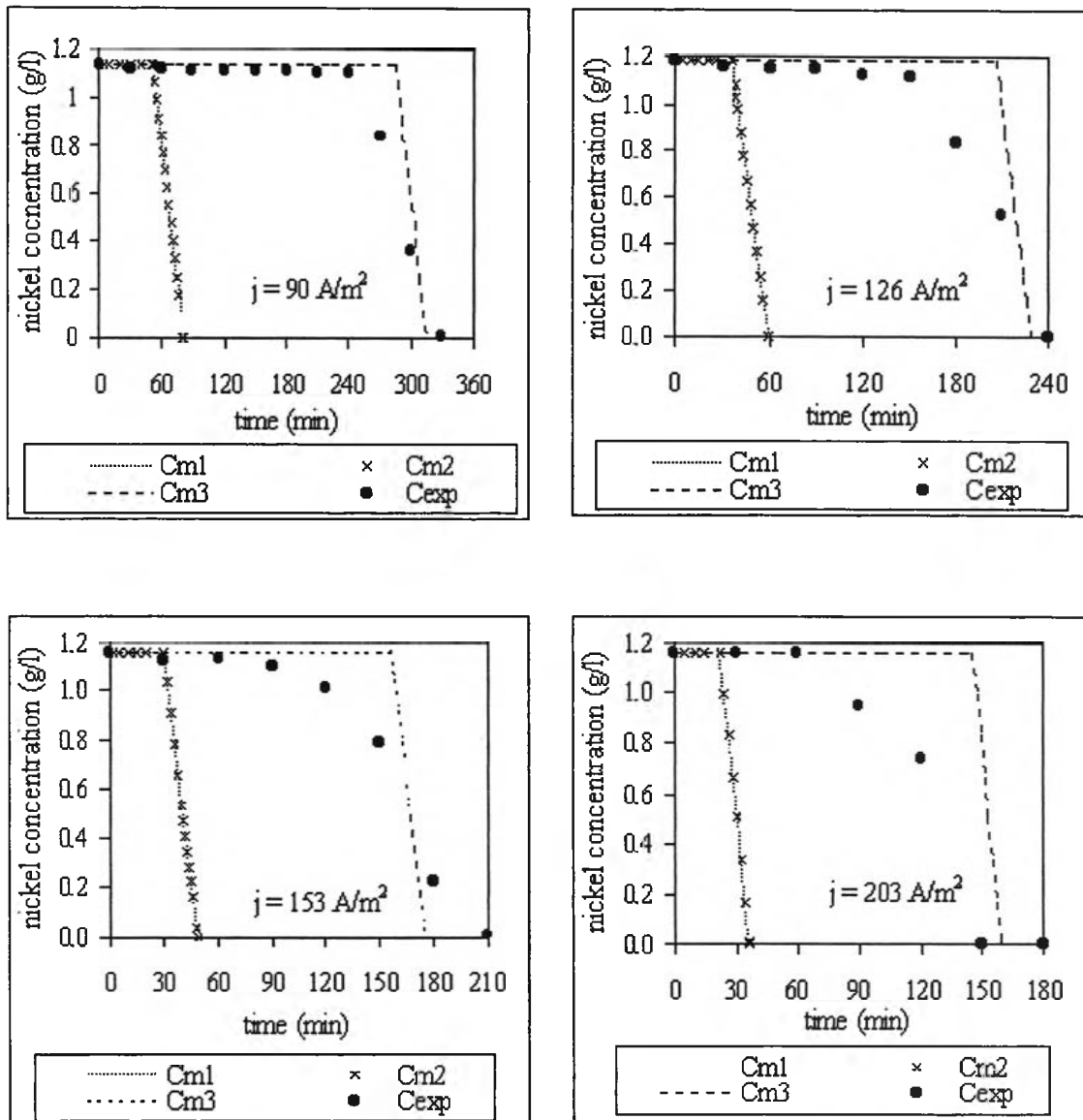


Figure V.35: Plots of C_{m1} , C_{m2} , C_{m3} and C_{exp} evolution versus time (solution S8).

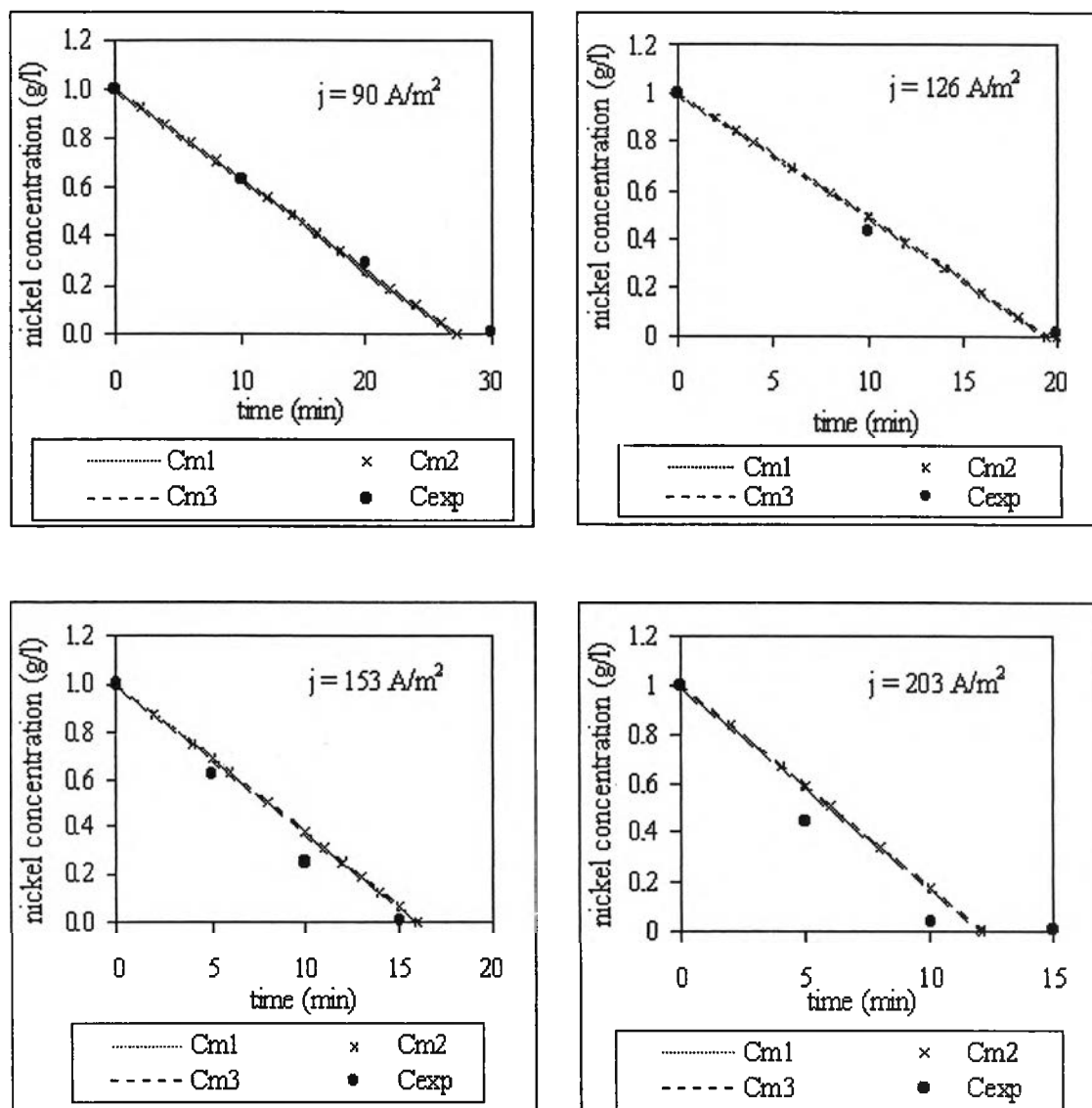


Figure V.36: Plots of C_{m1} , C_{m2} , C_{m3} and C_{exp} evolution versus time (solution S9).

For high initial concentration solutions, experiments have been performed by synthetic nickel solutions with concentration of 10 g/l, pH = 1 (solution S10) and 10 g/l at pH = 5 (solution S11) at current density of 90 and 203 A/m^2 . Figures V.37 and V.38 respectively show the plots of percentage of nickel recovery, the pH evolution in anodic and cathodic compartments versus electrolysis time of solution S10 and solution S11.

For low initial pH solution (solution S10), nickel was completely recovered in 8.5 and 5 hours at current density of 90 and 203 A/m^2 , respectively. When pH

solution is lower than precipitation pH, the nickel deposition occurred which can be observed from the increasing of nickel recovery percentage.

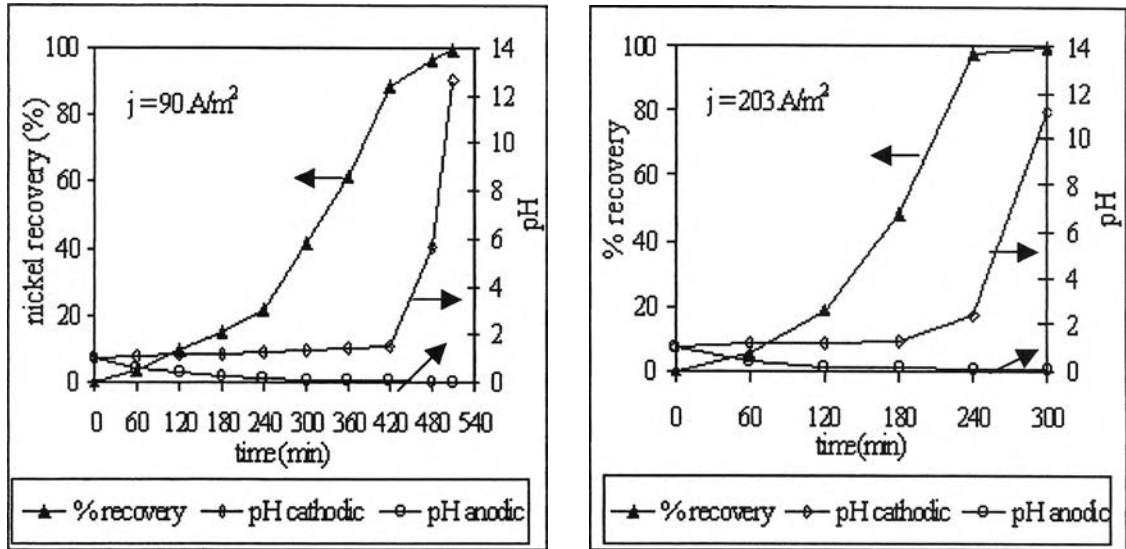


Figure V.37: Nickel recovery percentage and pH versus time (solution S10).

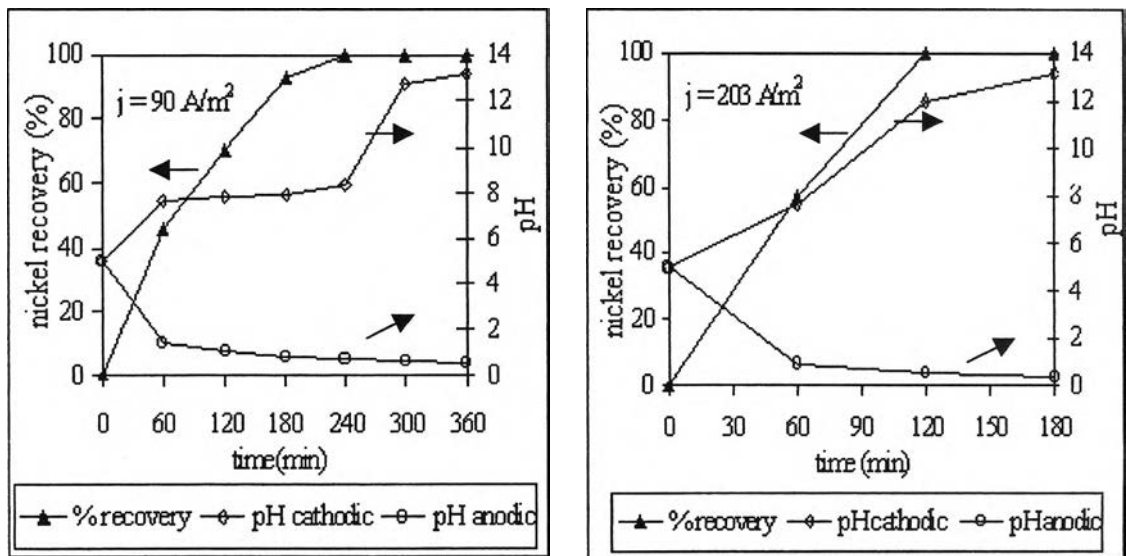


Figure V.38: Nickel recovery percentage and pH versus time (solution S11).

For solution S11, nickel was completely recovered after 4 and 2 hours at current density of 90 and 203 A/m^2 , respectively. Considering at current density of 90 A/m^2 , the constant pH in cathodic compartment at $\text{pH} \approx 7.9$ was observed, this region corresponds to the nickel precipitation. The nickel deposition didn't observed at this

pH solution because the nickel precipitation occurred quickly due to high amount of hydroxide ions in solution.

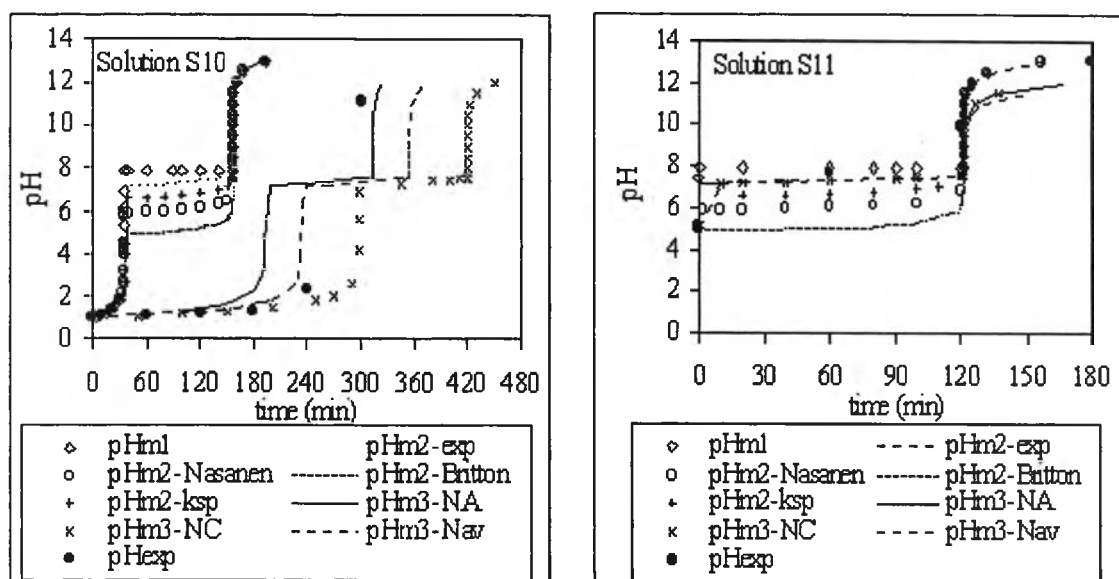


Figure V.39: Plots of pH_{m1} , pH_{m2} , pH_{m3} and pH_{exp} evolution versus time at 203 A/m^2 (solutions S10 and S11).

Figure V.39 shows the summation plots of pH evolution versus electrolysis time of nickel solution (solution S10 and S11) at current density of 203 A/m^2 . The results showed the similar tendency as solutions S8 and S9 in that the third model gave the best fitting between experimental and model pH evolutions. The loss flux of hydroxide ions had strong effect on the low initial pH solution whereas it had no effect on high initial pH solution.

2.3 Influence of initial pH and initial concentration

The effect of initial pH solution at current density of 203 A/m^2 is shown in Figure V.40, solutions with high initial pH had lower electrolysis time about 10 and 2.5 times respectively for solution $\text{pH} = 1$ and $\text{pH} = 5$. This is due to the high initial pH solution having small amount of proton. So, it uses only short time to reduce the quantity of protons and nickel ions precipitate faster than in lower initial pH solution.

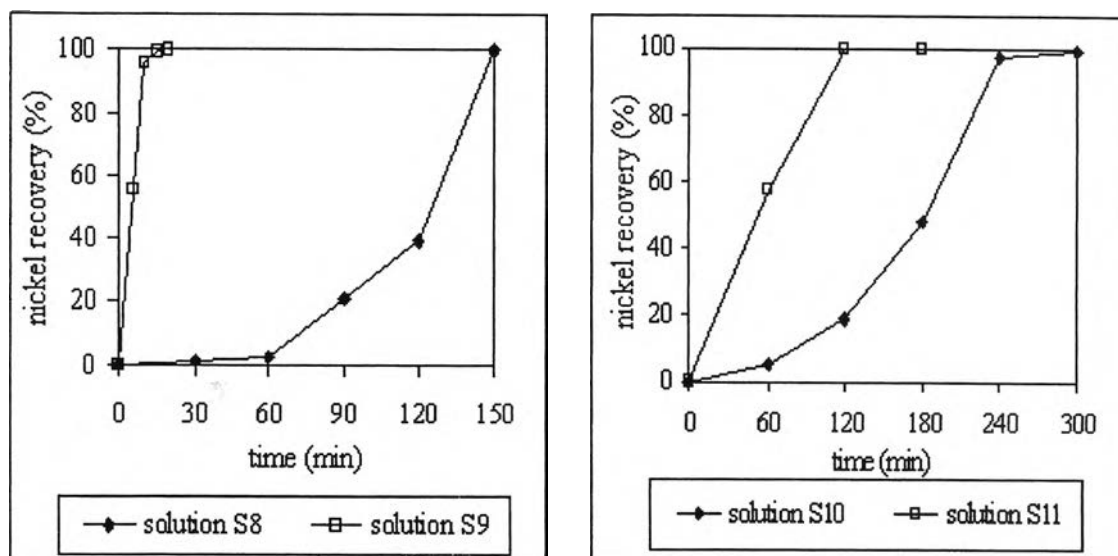


Figure V.40: Effect of initial pH on nickel recovery versus time at 203 A/m^2 .

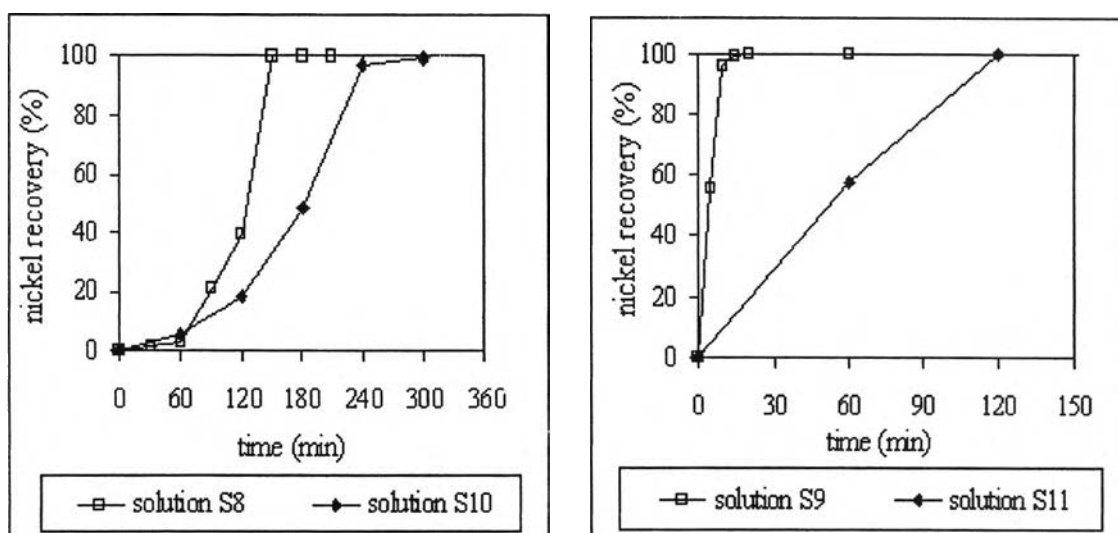


Figure V.41: Effect of initial concentration on nickel recovery versus time at 203 A/m^2 .

Figure V.41 shows the plots of percentage of nickel recovery as a function of electrolysis time. Solution S8 needed a complete processing time approximately 150 minutes and solution S10 used processing time in 300 minutes. On the other hand, solution S9 had complete recovery time around 6 times faster than solution S11. It indicates that the complete recovery time is depending upon the initial concentration and solution pH. However, it isn't direct proportion between initial nickel concentration to electrolysis time or between initial pH to electrolysis time.

3. Conclusion

Chromium and nickel were recovered in reactor with anionic membrane by electroprecipitation technique in a range of current density of 90 - 203 A/m². The initial concentration of chromium and nickel were about 1 g/l and 10 g/l at pH = 1 and pH = 4.6–5. H₂SO₄ and NaOH were used to adjust the pH of solution to the preferable value and Na₂SO₄ (5 % wt) was used to keep the solution conductivity in the range of 20 - 40 mS/cm.

From the experimental work, it was found that both chromium and nickel ions were completely recovered at all current densities. Increasing current density causes decreasing electrolysis time. The most important parameter to this experiment is the operating cost which is calculated from electricity consumption in each experiment. It was focused that the optimum current density for both metals was found at 90 A/m². Operating costs were about 3.23 US\$/m³ and 0.72 US\$/m³ for chromium solutions at pH = 1 and pH = 4.6, respectively. For pH = 1 and pH = 5 of nickel solutions, the operating costs were about 4.42 US\$/m³ and 0.48 US\$/m³.

In order to predict the pH evolution in cathodic compartment, three models with different assumptions were developed. The total electrolysis time was separated into three zones depending on the observed reactions. The first zone depicts pH evolution from initial pH to precipitation pH. The second zone shows pH evolution during metal precipitation and the last zone concerns the evolution of pH after a complete metal precipitation is reached.

The results showed that the model with loss flux of hydroxide ions from cathodic to anodic compartments gave the best fitting with the experimental pH evolution for both low and high initial pH solution and initial concentration. This loss flux of hydroxide ions has strong effect on low initial pH solution while it has no effect on high initial pH solution. The reason should be that the loss of hydroxide ions is mainly observed during the first zone of electrolysis time and this loss depends upon the latent time. The low initial pH solution uses long electrolysis time to increase pH of solution from initial pH to precipitation pH, so the large amount of hydroxide ions transfer from cathodic compartment to anodic compartment.

By using the electroprecipitation process in industry, the operation should be performed with high initial pH solution in order to reduce the operating time and

operating cost. However, the other factors should be considered carefully such as metal ionic forms presented in solution, impurities or contaminants.